

Electronic Supplementary Information (ESI)

Polycyclic Heteroaromatic Hydrocarbons Containing a Benzoisoindole Core

Marcus Richter,^a Karl Sebastian Schellhammer,^b Peter Machata,^c Gianaurelio Cuniberti,^b
Alexey Popov,^c Frank Ortmann,^b Reinhard Berger,^{a,*} Klaus Müllen,^d and Xinliang Feng^{a,*}

*Corresponding Author. E-mail: xinliang.feng@tu-dresden.de and reinhard.berger@tu-
dresden.de

Table of Content

- 1) Experimental Section
- 2) Cyclic Voltammetry
- 3) UV-Vis Absorption Spectroscopy
- 4) Fluorescence Spectroscopy
- 5) DFT calculations
- 6) In Situ Electrochemistry
- 7) HR-MALDI-TOF Mass Spectrometry
- 8) NMR Spectroscopy
- 9) References

General Information

Unless otherwise stated, the commercially available reagents and dry solvents were used without further purification. The reactions were performed using standard vacuum-line and Schlenk techniques, work and purification of all compounds were performed under air and with reagent-grade solvents. Column chromatography was done with silica gel (particle size 0.063-0.2 mm from VWR) and silica coated aluminum sheets with fluorescence indicator from Merck were used for thin layer chromatography. Purification by recycling gel permeation chromatography (rGPC) was performed on JAI HPLC LC 9110 II NEXTwith fraction collector FC-3310 and GPC columns 2H and 1H (connected in series). The rGPC was used with HPLC-grade chloroform at room temperature.

NMR Data were recorded on a Bruker AV-III 600 spectrometer operating at 600 MHz for ^1H and 151 MHz for ^{13}C with standard Bruker puls programs at room temperature. Chemical shifts δ are given in ppm relative to TMS, coupling constants J are given in Hertz. CD_2Cl_2 ($\delta(^1\text{H}) = 5.32$ ppm, $\delta(^{13}\text{C}) = 53.8$ ppm), $\text{C}_2\text{D}_2\text{Cl}_4$ ($\delta(^1\text{H}) = 5.91$ ppm, $\delta(^{13}\text{C}) = 74.2$ ppm) or $\text{C}_2\text{D}_6\text{OS}$ ($\delta(^1\text{H}) = 2.50$ ppm, $\delta(^{13}\text{C}) = 39.56$ ppm) were used as solvent, lock and internal standard.

HR-MALDI-TOF MS spectra were recorded on a Bruker Autoflex Speed MALDI-TOF MS (Bruker Daltonics, Bremen, Germany) with *trans*-2-[3-(4-*tert*-Butylphenyl)-2-methyl-2-propenyldiene]malononitrile (DCTB) as the matrix. The preparation for all samples was performed in solid state.

UV-Vis absorption spectroscopy was conducted on an Agilent Technologies Cary Series 5000 by using 10 mm optical-path quartz cell at room temperature. Unless otherwise noted, a concentration of 10^{-5} mol/l in DCM was used for absorption between 0.1 and 1 at the wavelength region of experimental interest. Solution fluorescence spectra were recorded on a Perkin Elmer Fluorescence Spectrometer LS 55 at room temperature. Solution fluorescence spectra were recorded in argon-purged solutions at concentrations of 10^{-5} mol/l in anhydrous DCM. All measurements were carried out in a 10 mm fluorescence quartz cell at room temperature. Cyclic Voltammetry was carried out on a CHI 760 E potentiostat (CH Instruments, USA) in a three-electrode cell in a DCM solution of tetrabutylammonium hexafluorophosphate ($n\text{Bu}_4\text{NPF}_6$) (0.1 M) with a scan rate of 75 mV/s at room temperature. All measurements were recorded in argon-purged solutions of **1a-c** in anhydrous DCM. A Pt wire, Ag/AgCl (3M KCl solution), and a glassy carbon electrode were used as the counter electrode, the reference

electrode, and the working electrode, respectively. The oxidation potential for ferrocene $E_{\text{Fe}/\text{Fe}^+}$ in DCM was observed at 0.44 eV

In situ EPR/vis–NIR spectroelectrochemical experiments were performed in the optical EPR cavity (ER 4104OR, Bruker Germany). EPR spectra were recorded by the EMX X-band CW spectrometer (Bruker, Germany). Vis–NIR spectra were measured using the Avantes spectrometer AvaSpec-2048x14-USB2 with the CCD detector and AvaSpec-NIR256-2.2 with the InGaAs detector applying the AvaSoft 7.5 software. For electron excitation, halogen lamp Avantes Avalight-Hal-S was used. Both, the EPR spectrometer and the Vis–NIR spectrometer are linked to a HEKA potentiostat PG 390 which triggers both spectrometers. Triggering is performed by the software package PotMaster v2x40 (HEKA Elektronik, Germany). For standard in situ EPR/vis–NIR spectroelectrochemical experiments an EPR flat cell was used. A laminated platinum mesh as the working electrode, a silver wire as the pseudo-reference electrode, and a platinum wire as the counter electrode were used in spectroelectrochemical experiments. Concentrated 0.5 M TBAPF₆ supporting electrolyte was used to improve the electrochemical response in flat spectroelectrochemical cell with larger iR drop comparing to the conventional electrochemical cell.

1) Experimental Section

The synthesis of 8-(*tert*-butyl)dibenzo[*d,k*]naphtha[*a*]ullazine-1,6-dione **5** from commercially available 1,3-dibromo-*tert*-butyl aniline was reported previously.¹

Synthesis of 11-(*tert*-butyl)-5,17-bis((triisopropylsilyl)ethynyl)-5,17-dihydrobenzo[7,8]naphtho[2',3':1,2]indolizino[6,5,4,3-*def*]phenanthridine-5,17-diol

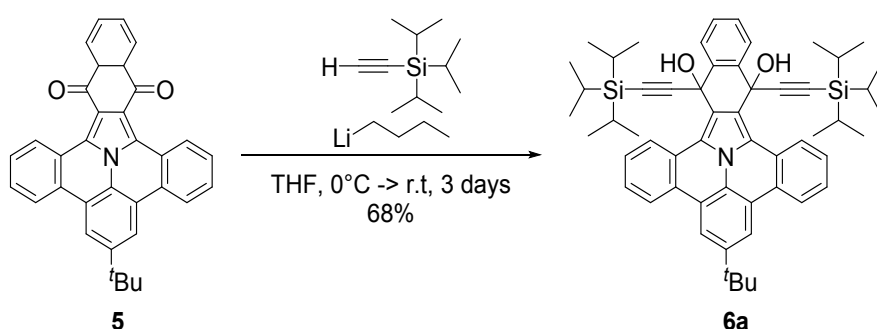
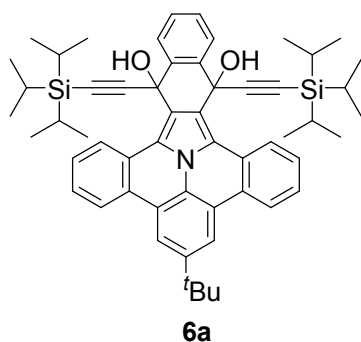


Figure S1. Synthesis of 11-(*tert*-butyl)-5,17-bis((triisopropylsilyl)ethynyl)-5,17-dihydrobenzo[7,8]naphtho[2',3':1,2]indolizino[6,5,4,3-*def*]phenanthridine-5,17-diol **6a**

In a dry and inert 25 ml Schlenk flask, 8-(*tert*-butyl)dibenzo[*d,k*]naphtha[*a*]ullazine-1,6-dione **5** (0.10 g, 0.20 mmol, 1.00 eq.) was suspended in anhydrous THF (4 ml, purged with argon). In a second dry and inert 25 ml Schlenk flask, (tri-*iso*-propylsilyl)acetylene (0.22 g, 1.26 mmol, 6.0 eq.) was dissolved in anhydrous THF (4 mL, purged with argon) and *n*-butyllithium (1.6 M in hexane, 1.34 mmol, 6.40 eq.) was added dropwise at 0°C . This sequence was repeated after 24 and 48 hours. Afterwards, stirring was continued for 24h and the reaction mixture was quenched with water and extracted with DCM (15 mL) three times. The combined organic layers were washed with brine and dried over magnesium sulfate. The solvent was removed under reduced pressure and the residue was purified by column chromatography on silica (hexane: ethyl acetate: 5:1). The crude product was purified by rGPC in chloroform to obtain compound **6a** as solid material (149 mg, 0.17 mmol, 68%).



¹H-NMR (600 MHz, DMSO-d₆): δ 9.78 – 9.77 (m, 2H), 8.66 (dd, *J* = 6.4 Hz, *J* = 3.4 Hz, 2H), 8.58 (s, 2H), 8.11 (dd, *J* = 6 Hz, *J* = 3.4 Hz, 2H), 7.59-7.57 (m, 4H), 7.49 – 7.48 (m, 2H), 6.82 (s, 2H), 1.57 (s, 9H), 0.87 (s, 18H), 0.86 (s, 18H), 0.79 (b, 6H)

¹³C-NMR (151MHz, DMSO-d₆): δ 147.10, 138.40, 129.82, 128.62, 127.75, 127.34, 127.02, 126.40, 125.47, 125.14, 122.44, 122.20, 120.97, 118.21, 117.77, 111.68, 63.53, 35.22, 31.47, 18.34, 18.20, 10.66

HR-MS (MALDI-TOF): *m/z* = 841.4749, calcd. for C₅₆H₆₇NO₂Si₂: *m/z* = 841.4710

HR-MALDI-TOF MS of the diol **6a** showed the exact molecular mass together. Partial disintegration was observed at an interval of *m/z* = 17, which hints at fragmentation of hydroxyl groups.

Synthesis of 11-(*tert*-butyl)-5,17-diphenyl-5,17-dihydrobenzo[7,8]naphtho[2',3':1,2]indolizino[6,5,4,3-def]phenanthridine-5,17-diol

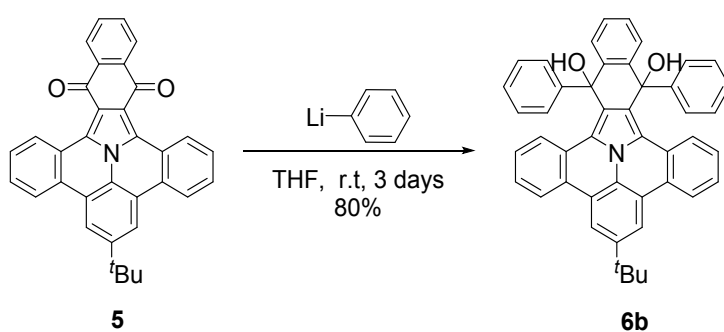
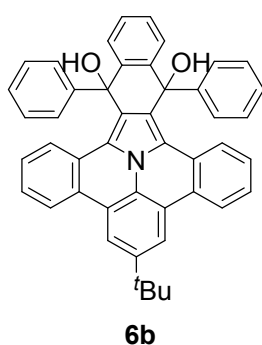


Figure S2. Synthesis of 11-(*tert*-butyl)-5,17-diphenyl-5,17-dihydrobenzo[7,8]naphtho[2',3':1,2]indolizino[6,5,4,3-def]phenanthridine-5,17-diol **6b**

In a dry and inert 25 ml Schlenk flask, 8-(*tert*-butyl)dibenzo[d,k]naphtho[a]ullazine-1,6-dione **5** (0.10 g, 0.20 mmol, 1.00 eq.) was suspended in anhydrous THF (4 mL, purged with argon) and phenyllithium (1.9 M in dibutylether, 1.25 mmol, 6.00 eq.) was added dropwise at room

temperature. The same addition of phenyllithium to the reaction mixture was repeated after 24h and 48 hours. Afterwards, stirring was continued for 24h and the reaction mixture was quenched with water and extracted with DCM (15ml) three times. The combined organic layers were washed with brine and dried over magnesium sulfate. The solvent was removed under reduced pressure and the residue was purified by column chromatography on silica (hexane: ethyl acetate: 5:1). The crude product was purified by rGPC in chloroform to obtain compound **6b** as solid material (0.106 mg, 0.16 mmol, 80%). Partial dihydroxylation was observed in NMR and MALDI-TOF MS. Since we believe, that this does not affect the further step the product was used without further purification.



¹H-NMR (600 MHz, DMSO-*d*₆): δ 9.34 – 9.33 (dd, *J* = 8.1 Hz, *J* = 1.3 Hz, 2H), 8.50 (b, 2H), 8.48 (b, 2H), 7.70 (b, 2H), 7.58 – 7.56 (m, 2H), 7.40 – 7.39 (m, 2H), 7.37 – 7.36 (m, 2H), 7.23 – 7.22 (m, 2H), 7.13-7.12 (m, 2H), 7.11 – 7.10 (m, 2H), 7.06 – 7.05 (m, 2H), 7.02 (s, 2H), 7.00 - 6.98 (m, 2H), 1.51 (s, 9H)

¹³C-NMR (151MHz, DMSO-*d*₆): δ 148.21, 147.20, 140.98, 128.91, 128.88, 127.66, 127.55, 127.28, 127.15, 126.65, 126.40, 125.98, 125.64, 125.11, 124.52, 122.44, 122.19, 122.11, 117.65, 71.34, 35.13, 31.41

HR-MS (MALDI-TOF): *m/z* = 633.2874, calcd. for C₄₆H₃₅NO₂: *m/z* = 633.2668

The NMR of **6b** showed further peaks which could not be assigned. We suspect partial dihydroxylation of the product. HR-MALDI-TOF measurement of the diol **6b** gave the exact mass. Partial disintegration was observed at an interval of *m/z* = 17, which hints at fragmentation of hydroxyl groups.

Synthesis of 5,17-bis(benzo[b]thiophen-2-yl)-11-(*tert*-butyl)-5,17-dihydrobenzo[7,8]naphtho[2',3':1,2]indolizino[6,5,4,3-def]phenanthridine-5,17-diol

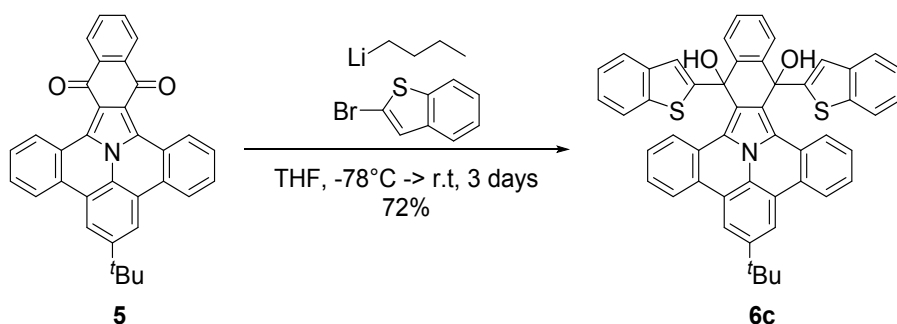
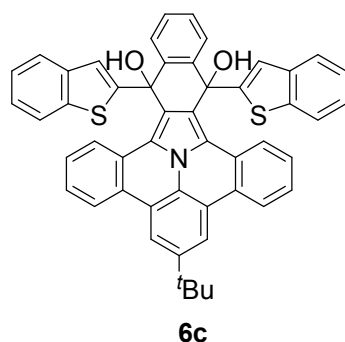


Figure S3. Synthesis of 5,17-bis(benzo[b]thiophen-2-yl)-11-(*tert*-butyl)-5,17-dihydrobenzo[7,8]naphtho[2',3':1,2]indolizino[6,5,4,3-def]phenanthridine-5,17-diol **6c**

In a dry and inert 25 ml Schlenk flask, 8-(*tert*-butyl)dibenzo[d,k]naphtha[a]ullazine-1,6-dione **5** (0.10 g, 0.20 mmol, 1.00 eq.) was suspended in anhydrous THF (4 mL, purged with argon). In a second dry and inert 25 ml Schlenk flask, 2-bromobenzothiophene (0.26 g, 1.26 mmol, 6.0 eq.) was dissolved in anhydrous THF (4 mL, purged with argon) and *n*-butyllithium (1.6 M in hexane, 1.34 mmol, 6.40 eq.) was added dropwise -78°C. This sequence was repeated after 24h and 48 hours. Afterwards, stirring for 24 hours and the reaction mixture was quenched with water and extracted with DCM (15 mL) three times. The combined organic layers were washed with brine and dried over magnesium sulfate. The solvent was removed under reduced pressure and the residue was purified by column chromatography on silica (hexane: ethyl acetate: 5:1). The crude product was purified by rGPC in chloroform to obtain compound **6c** as solid material (112 mg, 0.15 mmol, 72%).



¹H-NMR (600 MHz, DMSO-*d*₆): δ 9.54 – 9.53 (m, 2H), 8.57 – 8.54 (m, 2H), 8.51 (s, 2H), 8.08 (dd, *J* = 6 Hz, *J* = 3.4 Hz, 2H), 7.81 - 7.80 (m, 2H), 7.49 (s, 2H), 7.46 – 7.45 (m, 2H), 7.41 – 7.39

(m, 4H), 7.27 (dd, $J = 6.4$ Hz, $J = 3.4$ Hz, 2H), 7.18 – 7.16 (m, 4H), 7.04 (s, 2H), 1.52 (s, 9H)

$^{13}\text{C-NMR}$ (151MHz, DMSO-d_6): δ 155.39, 147.22, 139.91, 139.15, 138.76,, 128.85, 128.47, 127.41, 127.24, 126.99, 126.35, 125.40, 125.19, 123.98, 123.64, 123.17, 122.59, 122.22, 122.11, 121.32, 121.22, 117.70, 70.60, 35.16, 31.42

HR (MALDI-TOF): $m/z = 745.2113$, calcd. for $\text{C}_{50}\text{H}_{35}\text{NO}_2\text{S}_2$: $m/z = 745.2109$

HR-MALDI-TOF measurement of the diol **6c** showed the exact molecular mass. Partial disintegration was observed at an interval of $m/z = 17$, which hints at fragmentation of hydroxyl groups.

General procedure for the preparation of N-PAHs 1a-c

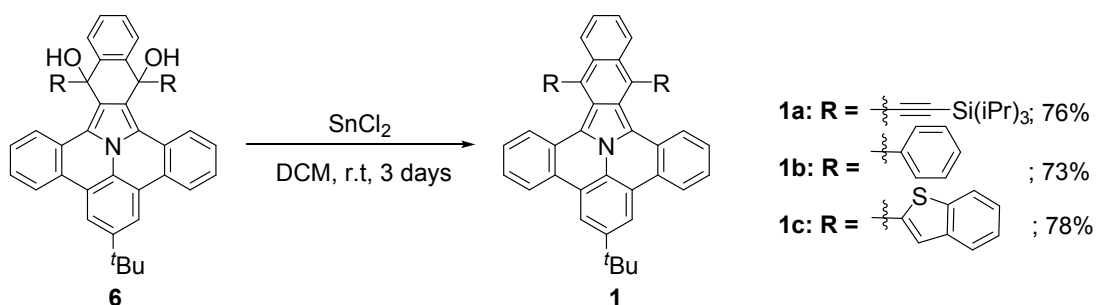
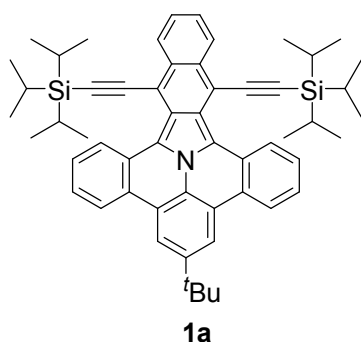


Figure S4. Synthesis of N-PAHs

The complete reactions and purification were carried out in the glovebox. In a dry and inert 25ml-Schlenk flask, precursor **6a-c** (0.1g, 1.00 eq.) and anhydrous SnCl_2 (7.00 eq.) were dissolved in anhydrous DCM (4 mL, purged with argon). Afterwards, the reaction mixture was stirred at room temperature for 3 days. After precipitation into cold methanol (100 mL, purged with argon) the title compound was filtered off and washed carefully. Yields are given in Figure S4.



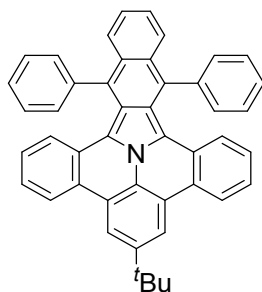
11-(*tert*-butyl)-5,17-bis((triisopropylsilyl)ethynyl)[7,8]naphtho[2,3':1,2]indolizino[6,5,4,3-def]phenanthridine

¹H-NMR (600 MHz, DCM-d₂): δ 9.22 (dd, *J* = 8.1 Hz, *J* = 0.9 Hz, 2H), 8.88 – 8.87 (m, 2H), 8.51 (s, 2H), 8.42 – 8.41 (m, 2H), 7.61 – 7.59 (m, 2H), 7.48 (ddd, *J* = 8.1 Hz, *J* = 7 Hz, *J* = 1.1 Hz, 2H), 1.60 (s, 9H), 1.25 – 1.21 (m, 6H), 1.13 (s, 18H), 1.11 (s, 18H).

¹³C-NMR (151MHz, DCM-d₂): δ 149.76, 133.07, 129.11, 127.97, 127.81, 127.56, 126.60, 125.90, 125.73, 125.57, 125.50, 122.74, 121.53, 117.51, 116.06, 111.75, 110.24, 106.00, 35.79, 31.77, 18.87, 11.81.

HR-MS (MALDI-TOF): *m/z* = 807.461, calcd. for C₅₆H₆₅NSi₂: *m/z* = 807.465

HR-MALDI-TOF MS gave the exact mass of **1a** and showed an additional peak plus *m/z* = 17 (OH-group). This can be attributed to partial oxidation during the MALDI-TOF measurement.



1b

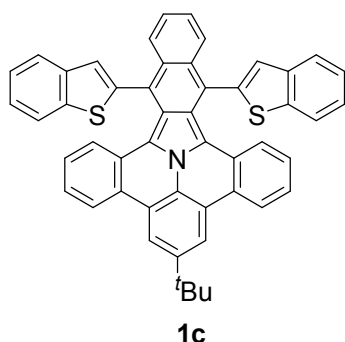
11-(*tert*-butyl)[7,8]-5,17-diphenylindolizino[6,5,4,3-def]phenanthridine

¹H-NMR (600 MHz, DCM-d₂): δ 8.44 (s, 2H), 8.29 (br dd, *J* = 8.1 Hz, *J* = 3.2 Hz, 2H), 8.19 – 8.16 (m, 2H), 7.69 – 7.66 (m, 2H), 7.53 – 7.50 (m, 4H), 7.49 – 7.46 (m, 2H), 7.34 – 7.31 (m, 2H), 7.24 – 7.19 (m, 4H), 6.85 – 6.82 (m, 2H), 1.58 (s, 9H)

¹³C-NMR (151MHz, DCM-d₂): δ 149.41, 141.67, 132.75, 130.23, 129.03, 128.55, 128.04, 127.88, 127.05, 126.62, 126.40, 126.33, 125.67, 125.21, 124.44, 123.93, 122.31, 121.69, 117.30, 115.38, 35.68, 31.73

HR-MS (MALDI-TOF): *m/z* = 599.268, calcd. for C₄₆H₃₃N: *m/z* = 599.261

HR-MALDI-TOF MS gave the exact mass of **1b** and showed an additional peak plus *m/z* = 17 (OH-group). This can be attributed to partial oxidation during the MALDI-TOF measurement.



5,17-bis(benzo[b]thiophen-2-yl)-11-(*tert*-butyl)[7,8]naphtho[2',3':1,2]indolizino[6,5,4,3-def]phenanthridine

¹H-NMR (600 MHz, C₂D₂Cl₄): δ 8.54 – 8.52 (m, 2H), 8.35 (s, 2H), 8.19 (br d, *J* = 8.3 Hz, 2H), 7.83 – 7.82 (m, 2H), 7.74-7.72 (br d, *J* = 7.9, 2H), 7.69 (s, 2H), 7.54 – 7.52 (br d, *J* = 8.1 Hz, 2H), 7.38 – 7.35 (m, 2H), 7.31 – 7.29 (m, 2H), 7.05 (ddd, *J* = 8.7 Hz, *J* = 1.1 Hz, 2H), 6.53 (ddd, *J* = 8.2 Hz, *J* = 1.2 Hz, 2H)

¹³C-NMR (151MHz, C₂D₂Cl₄): δ 149.60, 141.26, 128.35, 127.62, 127.41, 126.65, 126.42, 125.59, 125.35, 125.19, 125.05, 124.79, 124.76, 124.20, 122.51, 122.22, 117.23, 35.70, 31.96

HR-MS (MALDI-TOF): *m/z* = 711.209, calcd. for C₅₀H₃₃NS₂: *m/z* = 711.205

Due to the low solubility in *d*₂-tetrachloroethane chemical shifts of ¹³C nuclei were derived from the HSQC or from HMBC experiments. Unfortunately, not all quaternary carbon atoms could be detected. HR-MALDI-TOF gave the exact mass of **1c** and showed an additional peak plus *m/z* = 17 (OH-group). This can be attributed to partial oxidation during the MALDI-TOF measurement.

General procedure for the one-electron oxidation to the radical cation

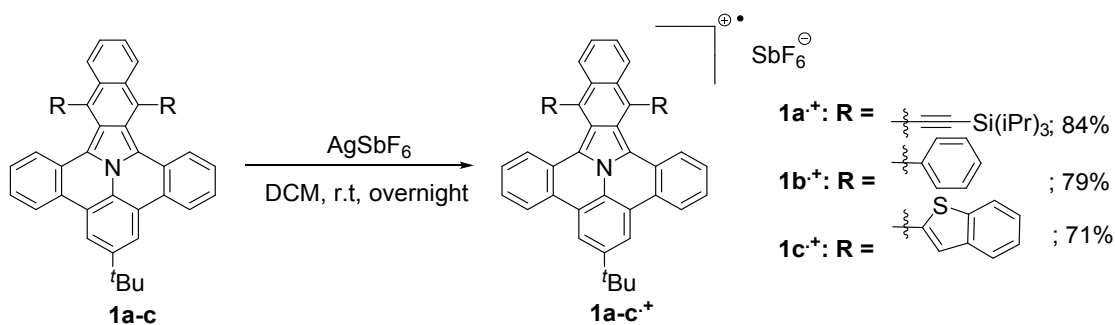
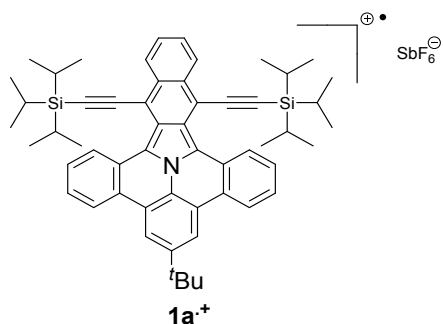


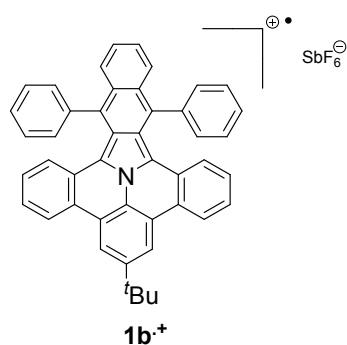
Figure S5. One-electron oxidation to **1a-c⁺**

The complete reaction and purification were carried out in the glovebox. In a dry and inert 25ml-Schlenk flask, the compounds **1a-c** (0.05g, 1.00 eq.) and AgSbF₆ (5.00 eq.) were dissolved in anhydrous DCM (4 mL, purged with argon) and stirred overnight. The reaction mixture was purified by short column chromatography on silica (anhydrous DCM, purged with argon) to afford the title compounds **1a-c**⁺. Yields are given in Figure S5.



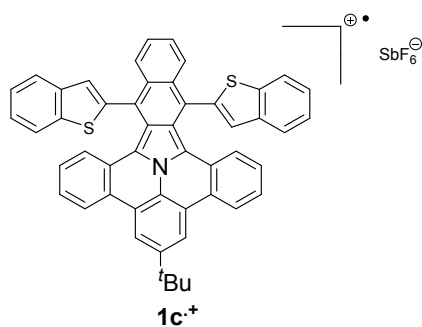
11-(*tert*-Butyl)-5,17-bis((tri-*iso*-propyl silyl)ethynyl)[7,8]naphtho[2',3':1,2]indolizino[6,5,4,3-def]phenanthridinium hexafluoroantimonate

HR-MS (MALDI-TOF): $m/z = 807.457$, calcd. for C₅₆H₆₅NSi₂: $m/z = 807.465$



11-(*tert*-Butyl)[7,8]-5,17-diphenylnaphtho[2',3':1,2]indolizino[6,5,4,3-def]phenanthridinium hexafluoroantimonate

HR-MS (MALDI-TOF): $m/z = 599.267$, calcd. for C₄₆H₃₃N: $m/z = 599.261$



5,17-Bis(benzo[b]thiophen-2-yl)-11-(*tert*-butyl)[7,8]naphtho[2',3':1,2]indolizino[6,5,4,3-def]phenanthridinium hexafluoroantimonate

HR-MS (MALDI-TOF): $m/z = 711.204$, calcd. for $C_{50}H_{33}NS_2$: $m/z = 711.205$

2) Cyclic Voltammetry

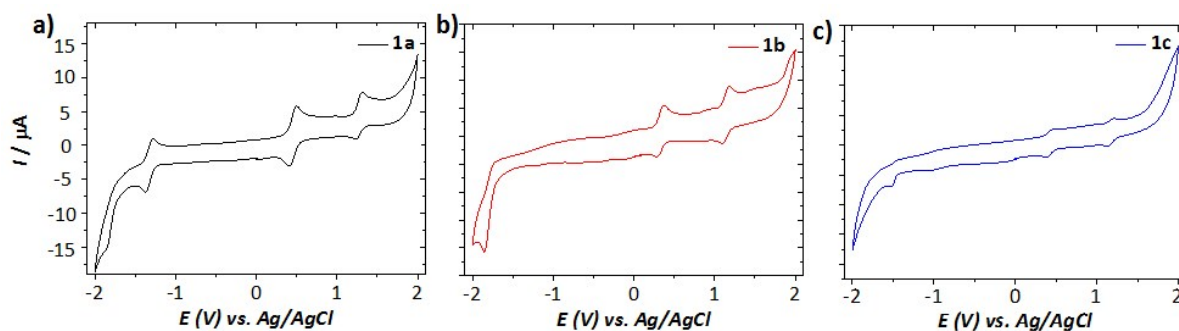


Figure S6. Cyclic voltammetry of 1a, 1b and 1c in potential range of -2 to 2 V in dry DCM with 0.1 M n-BuNPF₆ as supporting electrolyte.

Table S1. Oxidation and reduction potentials E^1_{ox} , E^2_{ox} , E^1_{red} and E^2_{red} (Ag/AgCl) obtained from onset potential in CV measurements. The experimental HOMO and LUMO levels were calculated using following equations:

$$E_{HOMO/LUMO} = -(4.8 + E^1_{ox/red} - E_{Fe/Fe+}).$$

	E^1_{ox} [V]	E^2_{ox} [V]	E^1_{red} [V]	E^2_{red} [V]	HOMO [eV]	LUMO [eV]
1a	0.45	1.27	-1.33	-1.84	-4.81	-3.03
1b	0.47	1.24	-1.85	-	-4.83	-
1c	0.41	1.20	-1.52	-	-4.77	-

3) UV-Vis Absorption Spectroscopy

General information

A dry and inert cuvette was charged with 2ml of a solution of **1a-c** ($10^{-5} \text{ mol l}^{-1}$ in argon purged DCM). Titration was performed by portionwise addition of AgSbF_6 or SbCl_5 (0.001 mol l^{-1} in argon purged DCM). UV-Vis spectra were recorded after every addition.

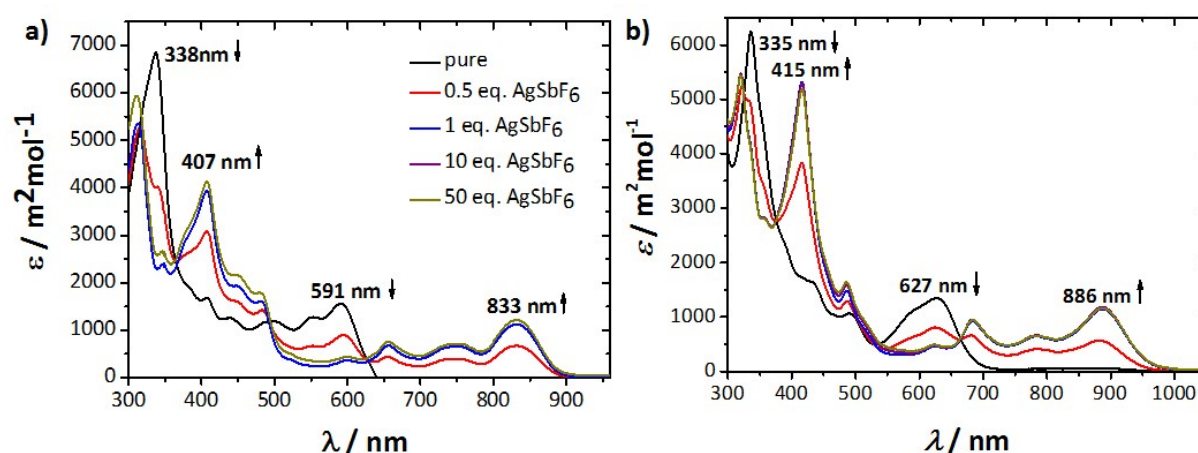


Figure S7. a) UV-Vis absorption titration spectra with AgSbF_6 of molecule **1b**; b) UV-Vis absorption titration spectra with AgSbF_6 of molecule **1c**

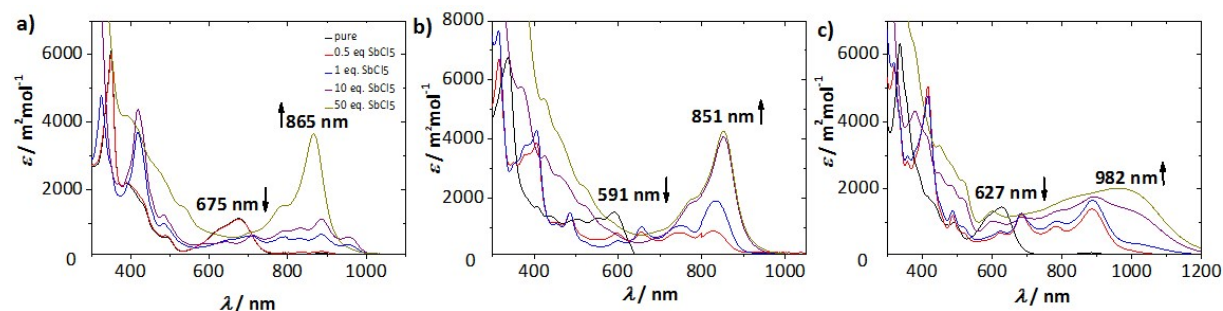


Figure S8. a) UV-Vis absorption titration spectra with SbCl_5 of molecule **1a**; b) UV-Vis absorption titration spectra with SbCl_5 of molecule **1b**; c) UV-Vis absorption titration spectra with SbCl_5 of molecule **1c**

Further UV-Vis titrations of **1a-c** were realized with antimony pentachloride (figure S8). The spectra with 0.5 eq. and 1 eq. SbCl_5 are similar to those obtained with AgSbF_6 (see Figure 5a, and S7). The addition of more than 10 eq SbCl_5 leads to broader peaks in the UV-Vis spectra which are not indications for dication species.

4) Fluorescence Spectroscopy

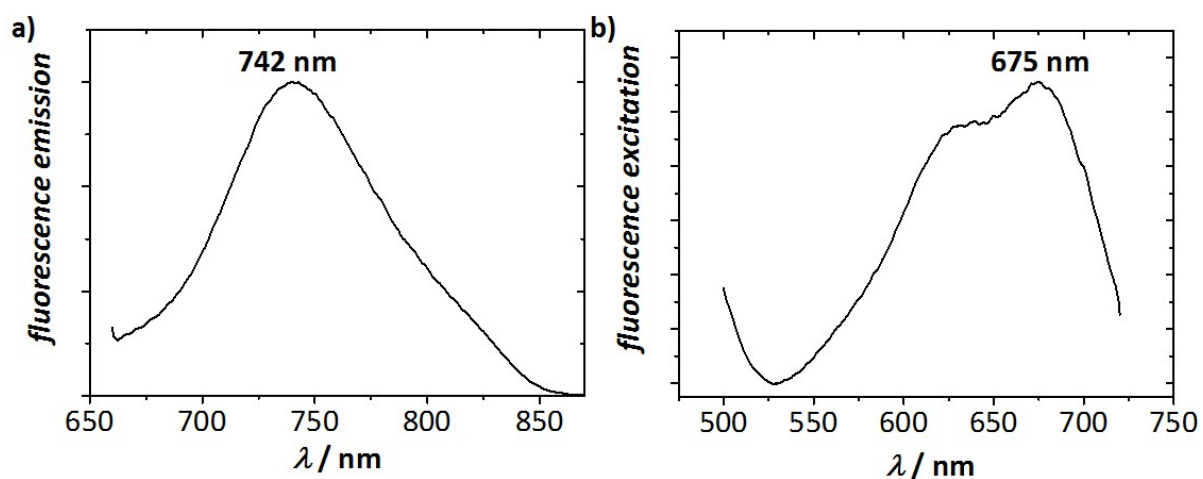


Figure S9: a) Fluorescence emission spectra of **1a** (measurements conditions: emission wavelength: 650 nm, gain: high, slit: 5 nm, speed 20 nm/min); b) Fluorescence excitation of **1a** (measurements conditions: excitation wavelength: 740 nm, gain: high, slit: 5 nm, speed 20 nm/min).

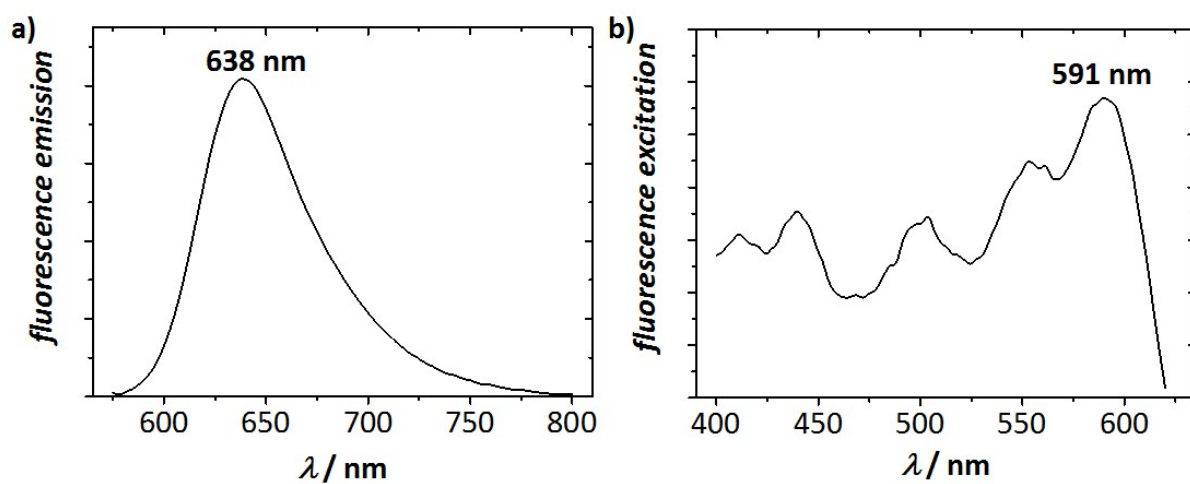


Figure S10. a) Fluorescence emission spectra of **1b** (measurements conditions: emission wavelength: 570 nm, gain: low, slit: 5 nm, speed 20 nm/min); b) Fluorescence excitation of **1b** (measurements conditions: excitation wavelength: 640 nm, gain: low, slit: 5 nm, speed 20 nm/min).

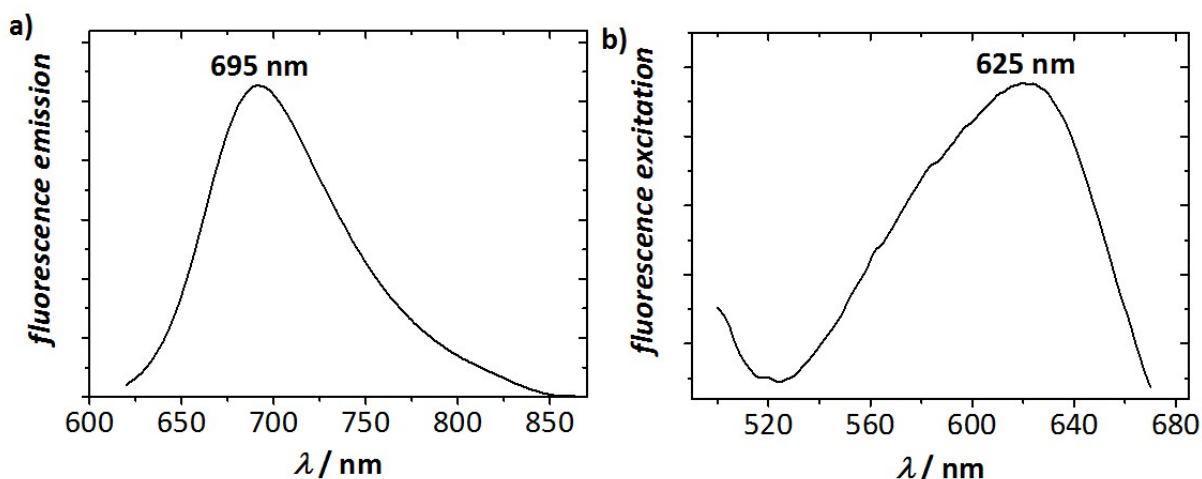


Figure S11. a) Fluorescence emission spectra of **1c** (measurements conditions: emission wavelength: 610 nm, gain: medium, slit: 5 nm, speed 20 nm/min); b) Fluorescence excitation of **1c** (measurements conditions: excitation wavelength: 690 nm, gain: medium, slit: 5 nm, speed 20 nm/min).

5) DFT calculations

Density functional theory (DFT) and time-dependent DFT (TD-DFT) simulations were performed within the Gaussian09 software package.² For structure relaxation and optical properties, the **spin-unrestricted** UCAM-B3LYP functional was used in combination with the 6-311G(d,p) basis set.^{3, 4} Hereby, absorption spectra of neutral and oxidized species were calculated based on the first 50 excited states using Gaussian-type linewidth broadening ($\sigma = 0.1$ eV) and an empirical polarization red-shift of 250 meV to account for solvent effects. The polarization-corrected values for the ionization potential (IP) and the electron affinity were calculated according to Ref.⁵ with the UCAM-B3LYP functional and the cc-pVTZ basis set. The singlet-triplet gap ΔE_{ST} was evaluated as

$$\Delta E_{ST} = E_S(q_S) - E_T(q_T), \quad (\text{S1})$$

with $E_S(q_S)$ and $E_T(q_T)$ the total energies of the singlet and triplet ground state, respectively, i.e., ΔE_{ST} denotes the minimum-to-minimum energy difference. To account for possible spin contamination of the open-shell singlet state by the first triplet state, the correction-scheme by Yamaguchi et al. was applied

$$E'_S(q_S) = E_S(q_S) - f \cdot \Delta E_{ST}^v \text{ with } f = \frac{{}^1\langle S^2 \rangle}{{}^3\langle S^2 \rangle - {}^1\langle S^2 \rangle}, \quad (\text{S2})$$

where ${}^1\langle S^2 \rangle$ and ${}^3\langle S^2 \rangle$ denote the expectation value of the square of the total spin operator

of the singlet and triplet state, respectively. ΔE_{ST}^v is the vertical singlet-triplet gap.^{6, 7} The diradical character \mathcal{Y} is evaluated from CASSCF(2,2)/6-311G** calculations by setting

$$y = 2D_{-1}^2, \quad (S3)$$

with D_{-1} the weight of the doubly excited configuration in the configuration-interaction expansion.⁸⁻¹⁸

As depicted in Fig. 12a, three stable conformers can be found for the phenyl-functionalized compound **1b**. The global energy minimum is found for a conformer with a twisted backbone. It reveals a very low open-shell character of $\mathcal{Y} = 0.08$ indicating that **1b** exhibits a closed-shell singlet ground state. Also within ambient conditions, the triplet state is not accessible with a minimum-to-minimum singlet-triplet gap of $\Delta E_{ST} = 1.23$ eV. In contrast, the energy minimum of the saddle conformer lies 35 meV above the twisted ground state and can be expected to be available in solution. Also this conformer features a closed-shell singlet state with similar values for \mathcal{Y} and ΔE_{ST} . The Y conformer, which lies 683 meV above the saddle conformer, has a weak open-shell singlet configuration with $\mathcal{Y} = 0.26$. Its spin density is depicted in Fig. S12c and shows delocalization of the unpaired electrons mostly over the naphthalene group and the phenyl side chains. However, due to the large energy difference it should be hardly accessible under ambient conditions. In addition, this conformer is only found for compound **1b**, while **1a** and **1c** exhibit energy minima only for the twisted and saddle conformer with the twisted conformer being always the global ground state. Consequently, all three compounds are showing a closed-shell singlet ground state.

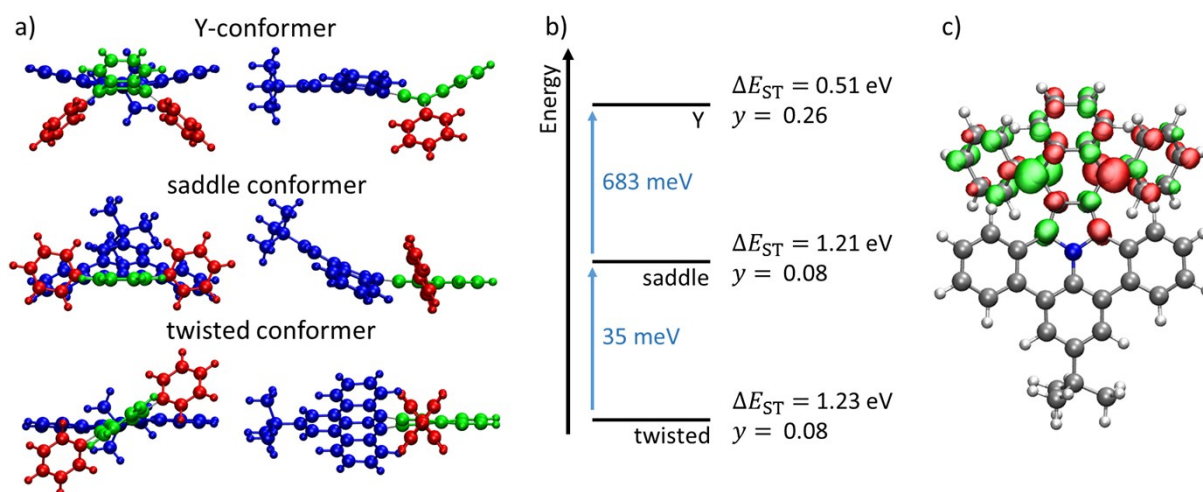


Figure S12. Characteristics of the three conformers of compound **1b**, ‘Y’, ‘saddle’ and ‘twisted’. (a) Structures of the conformers. For improved visibility, the naphthalene group is colored green, the phenyl side chains are colored red, and the head structure is colored blue. (b) Energy diagram and open-shell characteristics of the conformers. (c) Spin density of the open-shell singlet state of the Y-conformer.

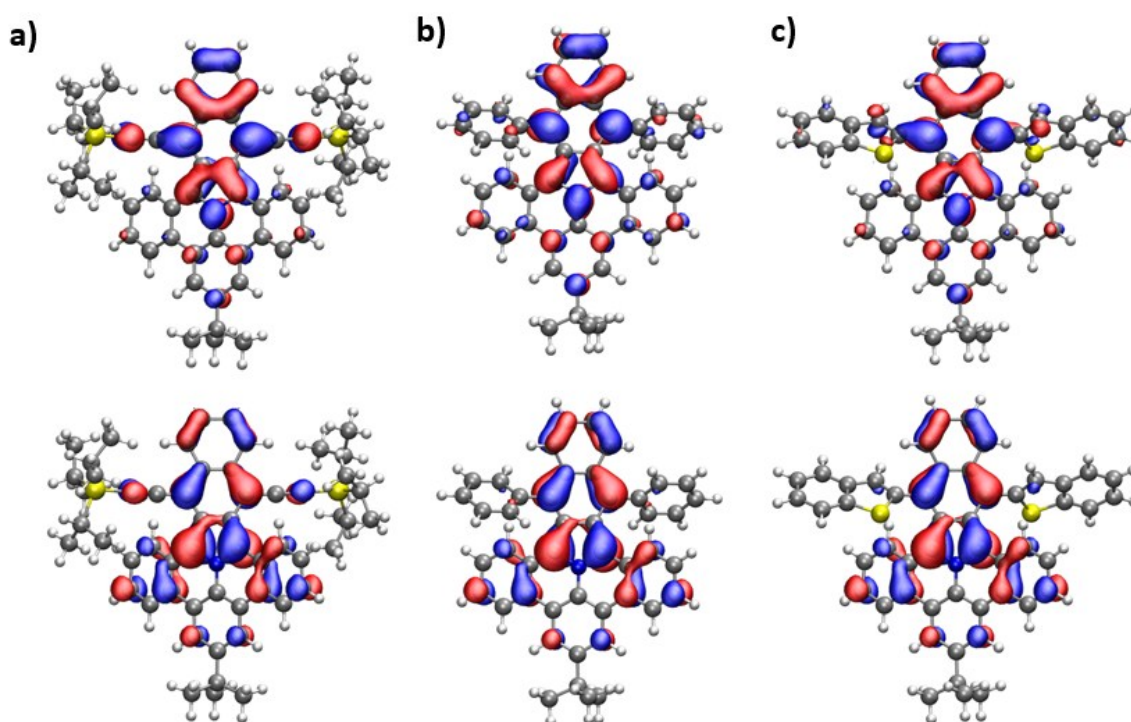


Figure S13. Graphical representation of LUMOs (top) and HOMOs (bottom) of **1a** (a) **1b** (b), and **1c** (c). The calculations were performed with DFT calculations based on the geometry of the twisted conformation. The LUMO and HOMO are partially localized at the benzoisindole core. The different substituents in 5- and 17-position as well as the *tert*-butyl group have no crucial influence on LUMO and HOMO. Remarkably, all HOMOs have a bisecting nodal plane through the 11-position and the nitrogen atom. Similar characteristics were observed for the HOMO and also the LUMO of **3**.¹

The presence of different conformers in solution even at room temperature is further supported by the experimental absorption spectra showing pronounced multi-peak structures which appear to go beyond simple vibrational features (Figure 4a, Figure 5b). Indeed, simulated absorption spectra obtained for the twisted and saddle conformer differ in a global bathochromic shift for the twisted conformer for compounds **1a-c** (Figure S14). This explains differences between experimental and simulated absorption spectra for the neutral and radical cation species. However, positions of absorption maxima can be accurately reproduced from TD-DFT simulations.

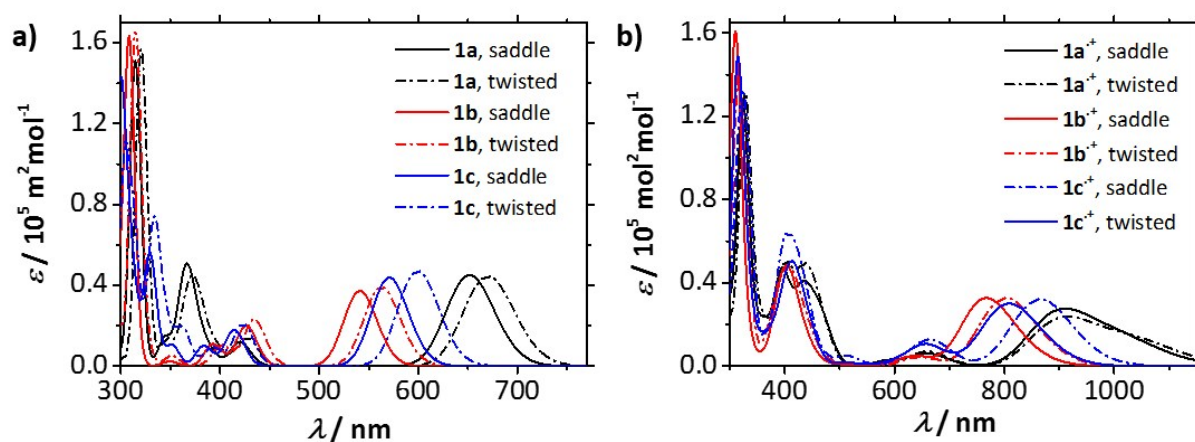


Figure S14. a) Simulation of the UV-Vis spectra of **1a-c** in twisted and saddle conformation; b) Simulation of the UV-Vis spectra of **1a-c⁺** in twisted and saddle conformation. For all compounds, twisted and saddle conformers show very similar optical and electronic properties with IP and EA varying by approximately 50 meV with the saddle conformer showing a slightly larger HOMO-LUMO gap as the twisted conformation. This leads to a slightly blue shifted absorption spectrum. Bathochromic shifts from **1b** to **1c** and **1a** can be related to push-pull-effects with the phenyl substituent being the weakest donor and TIPS showing pronounced delocalization of the frontier molecular orbitals in Fig. S13.

6) In situ Electrochemistry

General information

Experimental conditions of **1a** and **1c** in dichloromethane: scan rate 2.5 mV/s; $c = 2 \times 10^{-3}$ mol/L; EPR parameters: microwave power: 10.02 mW; modulation amplitude: 1 G; time constant: 20.48 ms, receiver gain: 40 dB; for well-defined spectrum modulation amplitude was decreased to 0.2 G.

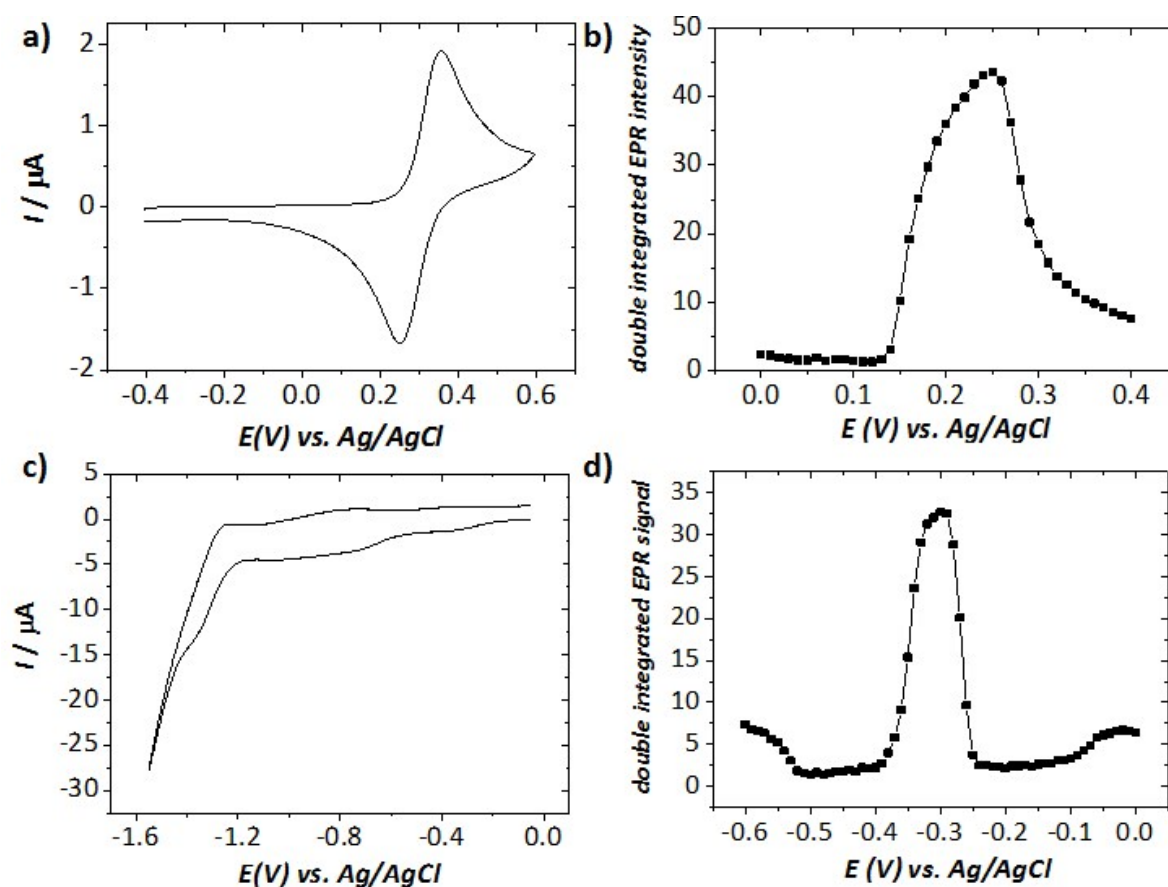


Figure S15. a) In situ cyclic voltammogram of **1a** of the first oxidation taken at a scan rate of 2.5 mV/s; b) Potential dependence of EPR double integral for **1a** of the first oxidation; c) In situ cyclic voltammogram of **1a** of the first reduction taken at a scan rate of 2.5 mV/s; d) Potential dependence of EPR double integral intensity for **1a** of the first reduction.

The g-factor for **1a^{•+}** was observed at 2.0025 obtained from the SEC in situ EPR measurement. For **1a^{•-}** the g-factor was measured at 2.0026.

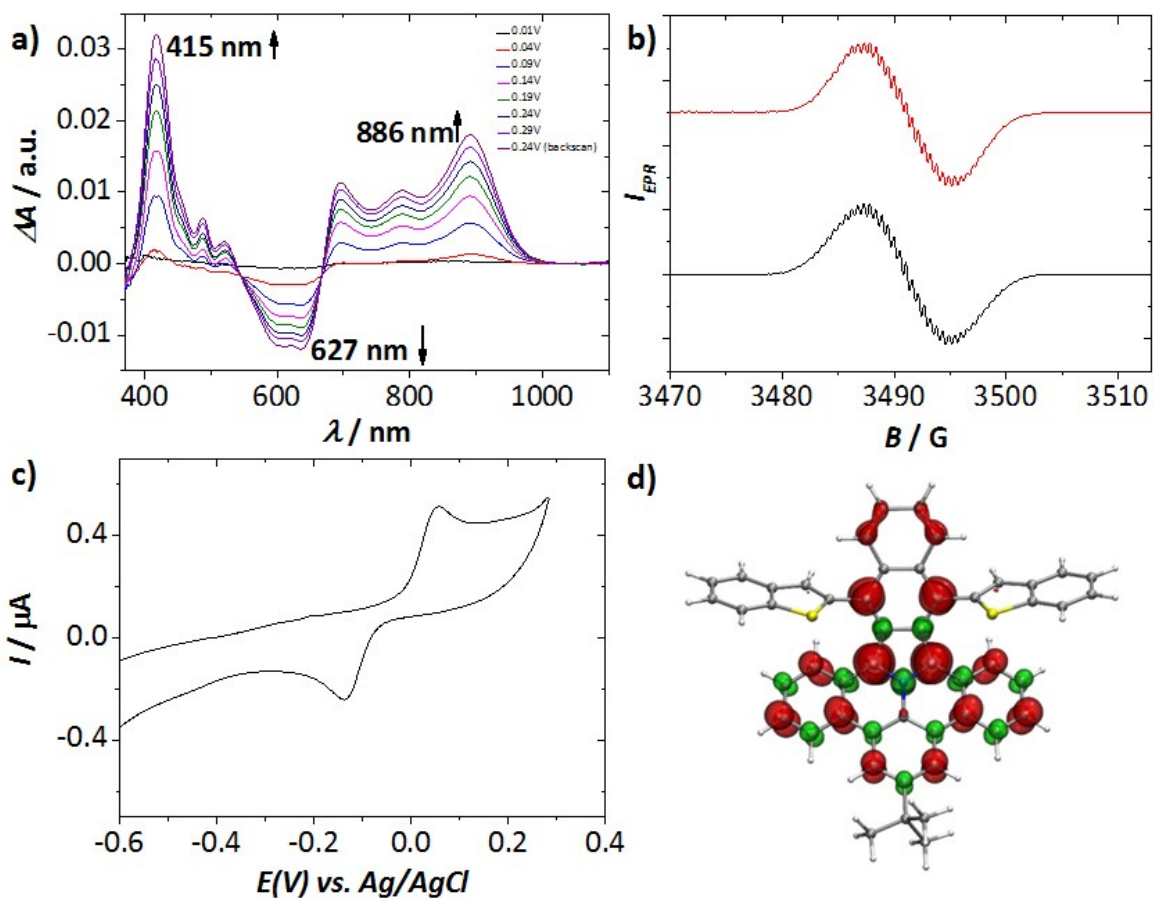


Figure S16. a) UV-Vis-NIR spectra at selected potentials observed during first oxidation of **1c**; b) EPR signal of **1c^{•+}** (black line: measurement and red line: simulation); c) In situ cyclic voltammogram of **1c** taken at a scan rate of 2.5 mV/s; d) DFT-computed spin density distribution of **1c^{•+}** (red" +", green" -").

From the SEC in situ EPR measurement, the g-factor of **1c^{•+}** was observed at 2.0024.

7) HR-MALDI-TOF Mass Spectrometry

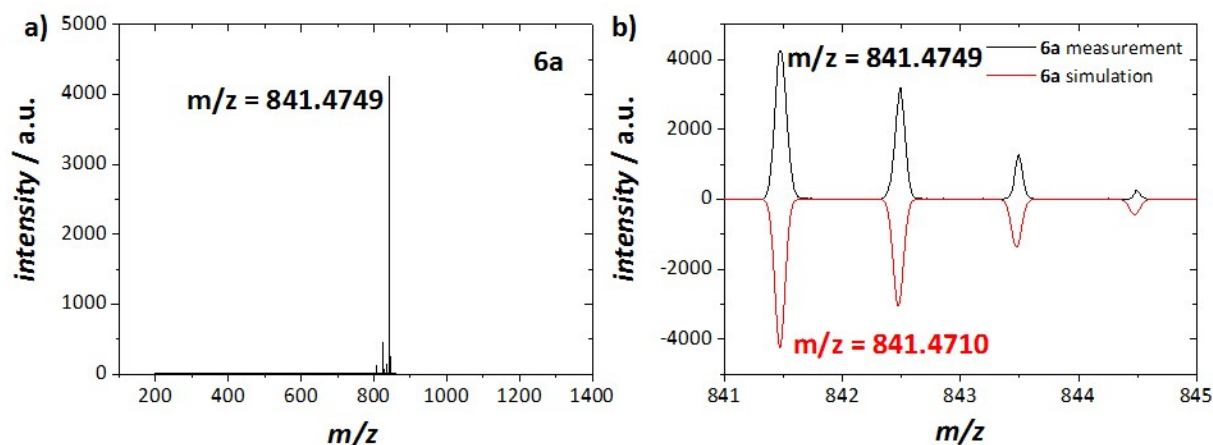


Figure S17. a) HR-MALDI-TOF spectrum of **6a**; b) HR-MALDI-TOF measurement of **6a** (black line) is in agreement to the expected isotopic distribution pattern (red line).

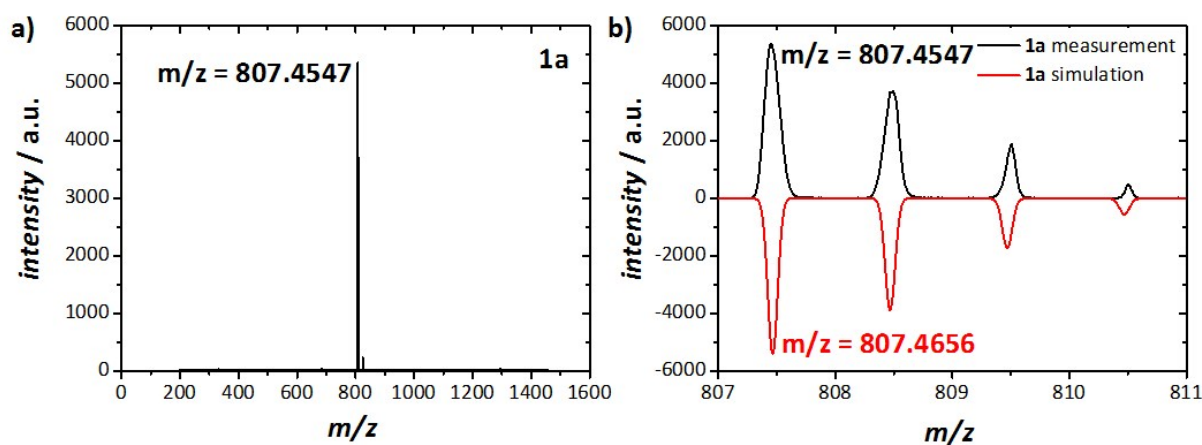


Figure S18. a) HR-MALDI-TOF spectrum of **1a**; b) HR-MALDI-TOF measurement of **1a** (black line) is in agreement to the expected isotopic distribution pattern (red line).

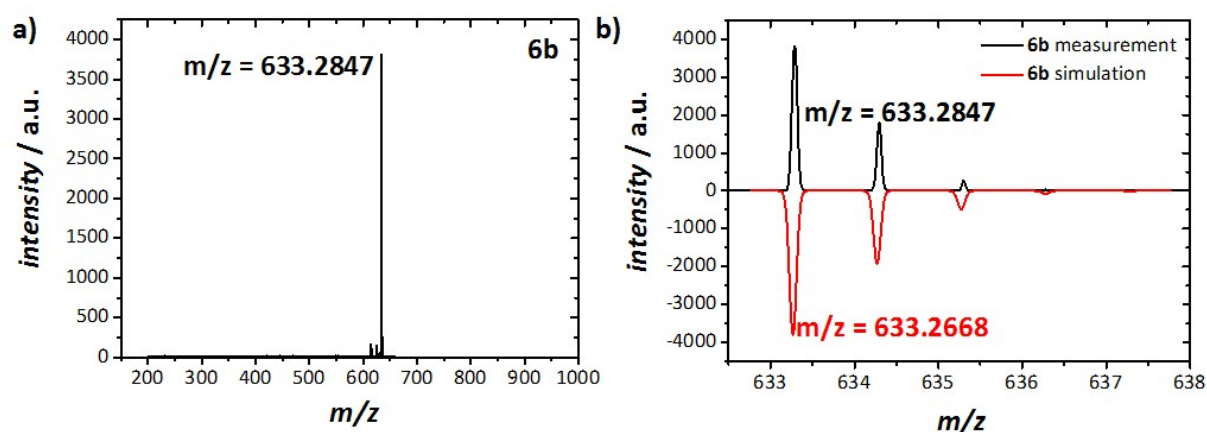


Figure S19. a) HR-MALDI-TOF spectrum of **6b**; b) HR-MALDI-TOF measurement of **6b** (black line) is in agreement to the expected isotopic distribution pattern (red line).

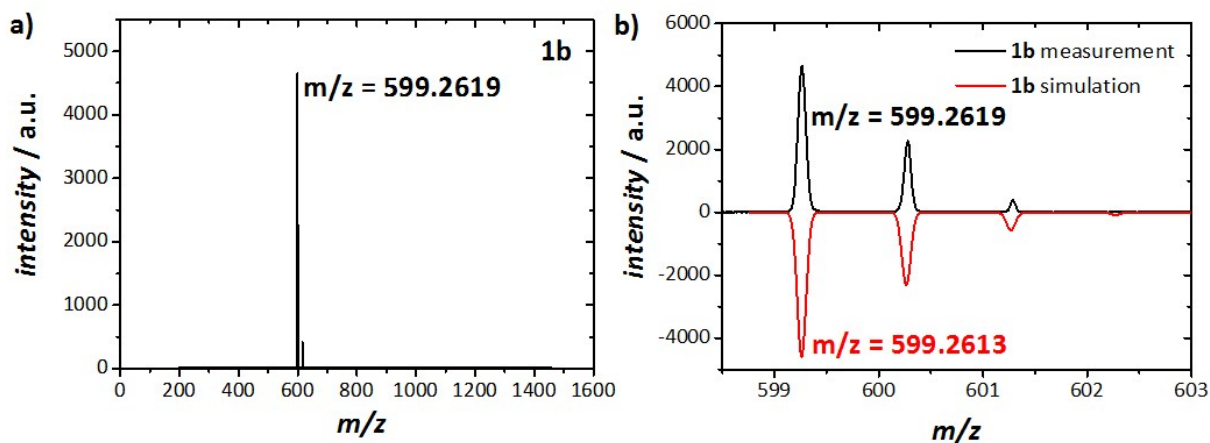


Figure S20. a) HR-MALDI-TOF spectrum of **1b**; b) HR-MALDI-TOF measurement of **1b** (black line) is in agreement to the expected isotopic distribution pattern (red line).

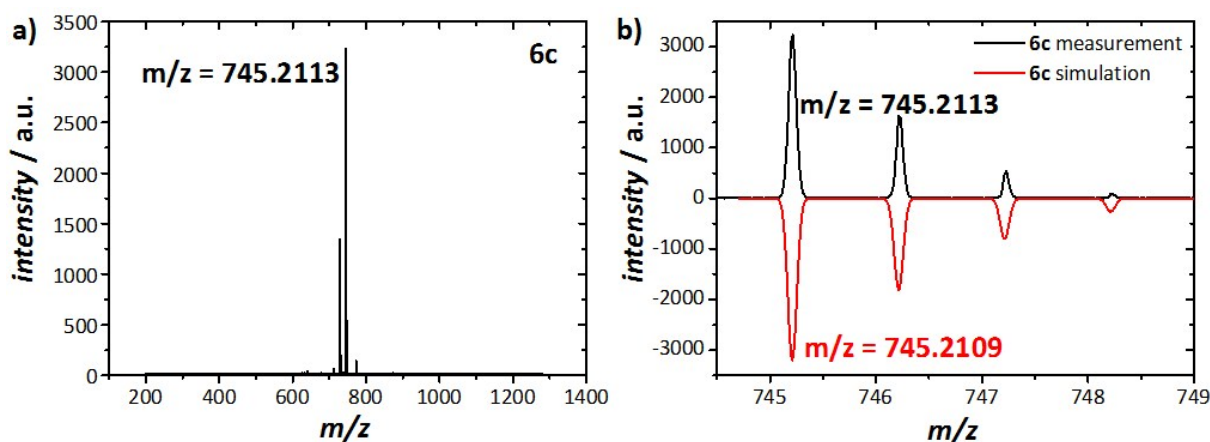


Figure S21. a) HR-MALDI-TOF spectrum of **6c**; b) HR-MALDI-TOF measurement of **6c** (black line) is in agreement to the expected isotopic distribution pattern (red line).

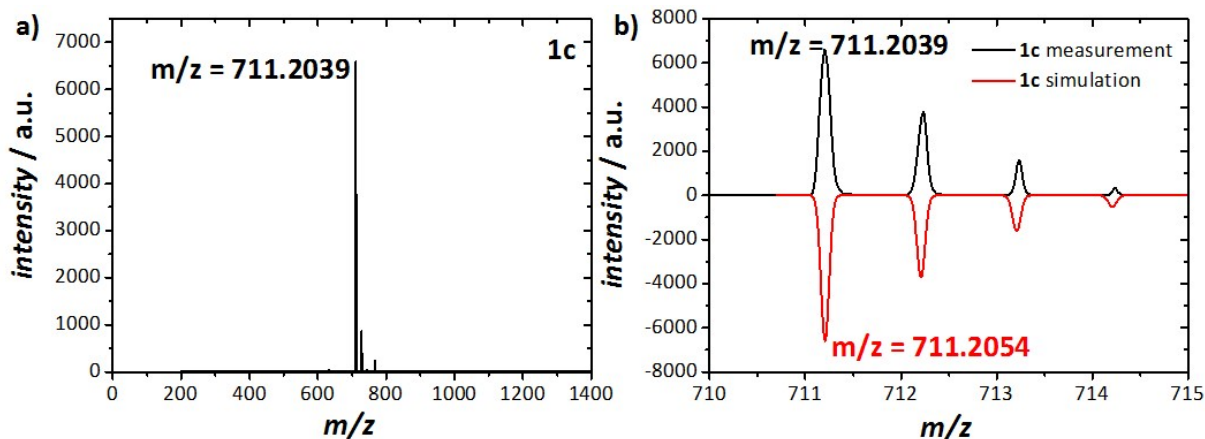


Figure S22. a) HR-MALDI-TOF spectrum of **1c**; b) HR-MALDI-TOF measurement of **1c** (black line) is in agreement to the expected isotopic distribution pattern (red line).

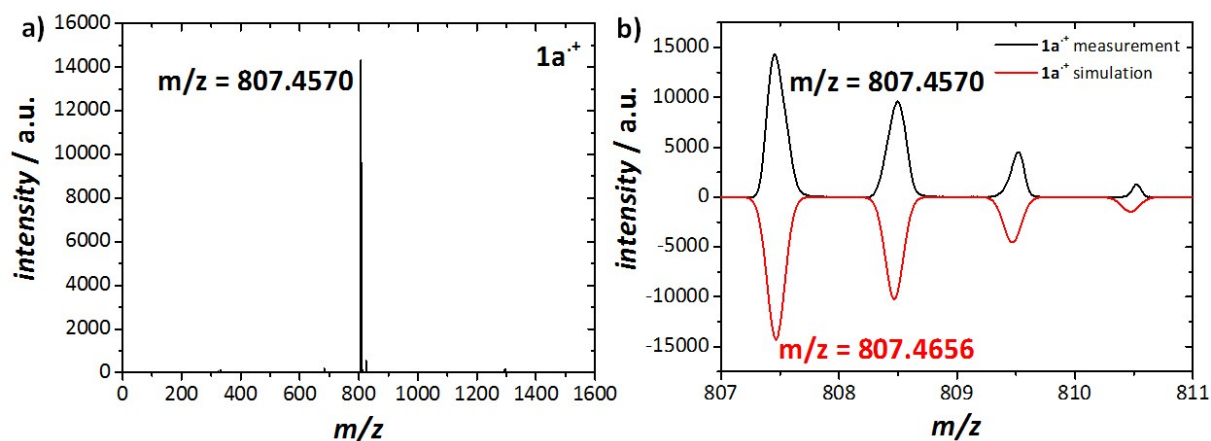


Figure S23. a) HR-MALDI-TOF spectrum of $1a^+$; b) HR-MALDI-TOF measurement of $1a^+$ (black line) is in agreement to the expected isotopic distribution pattern (red line).

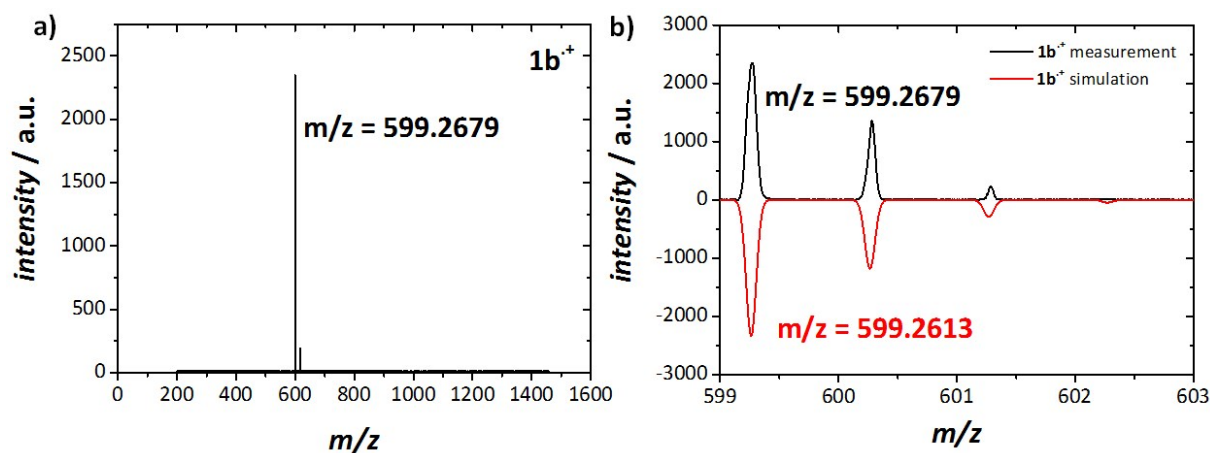


Figure S24. a) HR-MALDI-TOF spectrum of $1b^+$; b) HR-MALDI-TOF measurement of $1b^+$ (black line) is in agreement to the expected isotopic distribution pattern (red line).

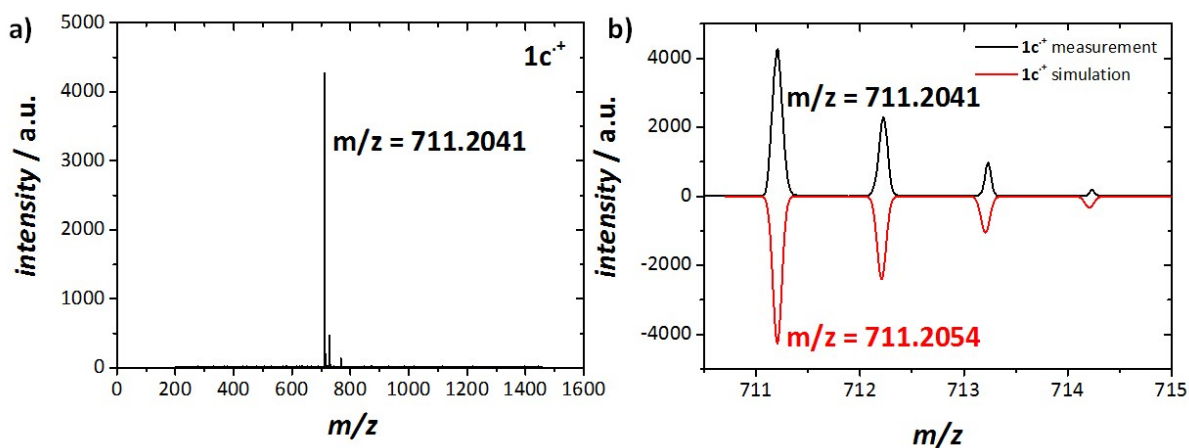
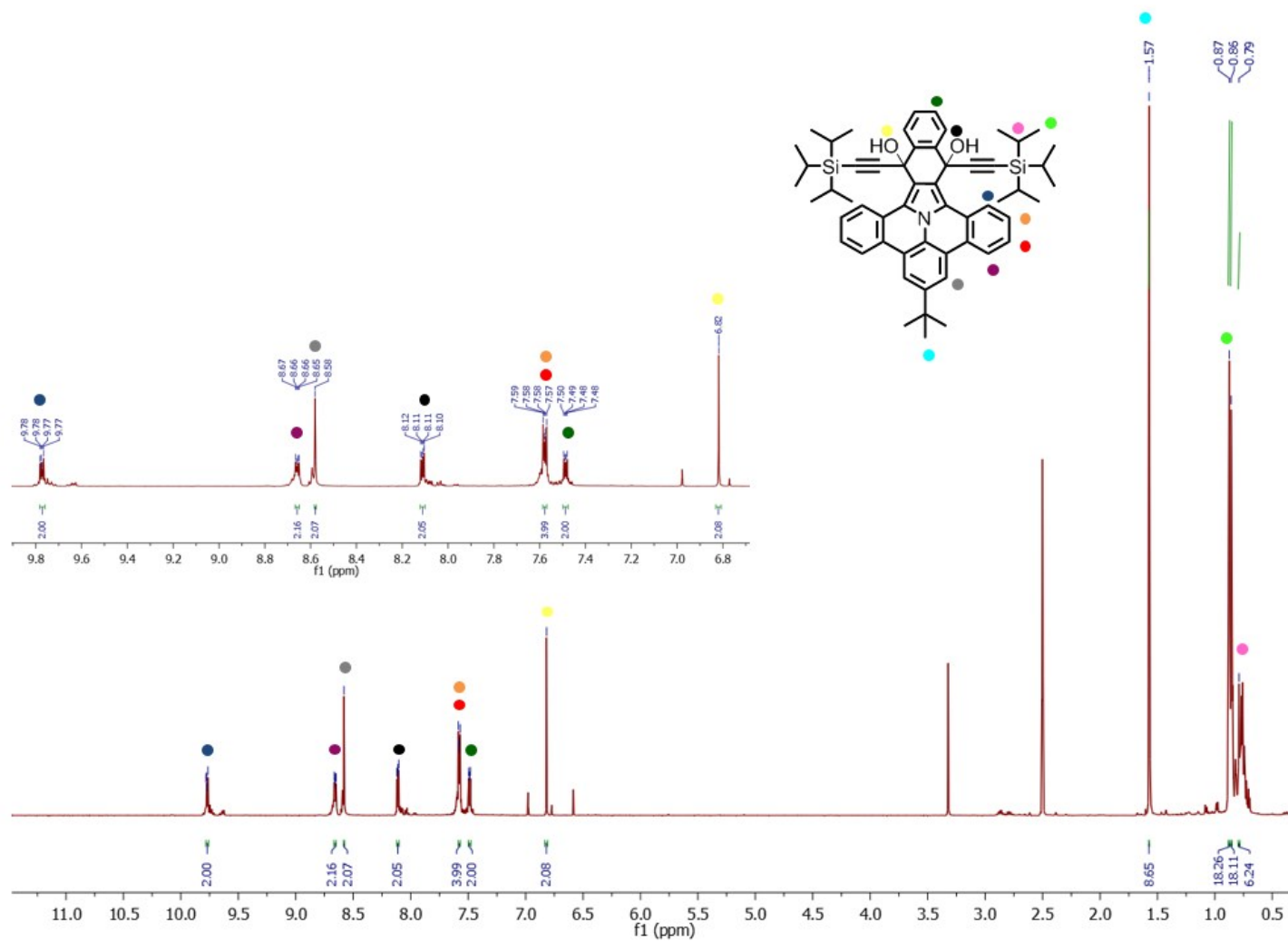
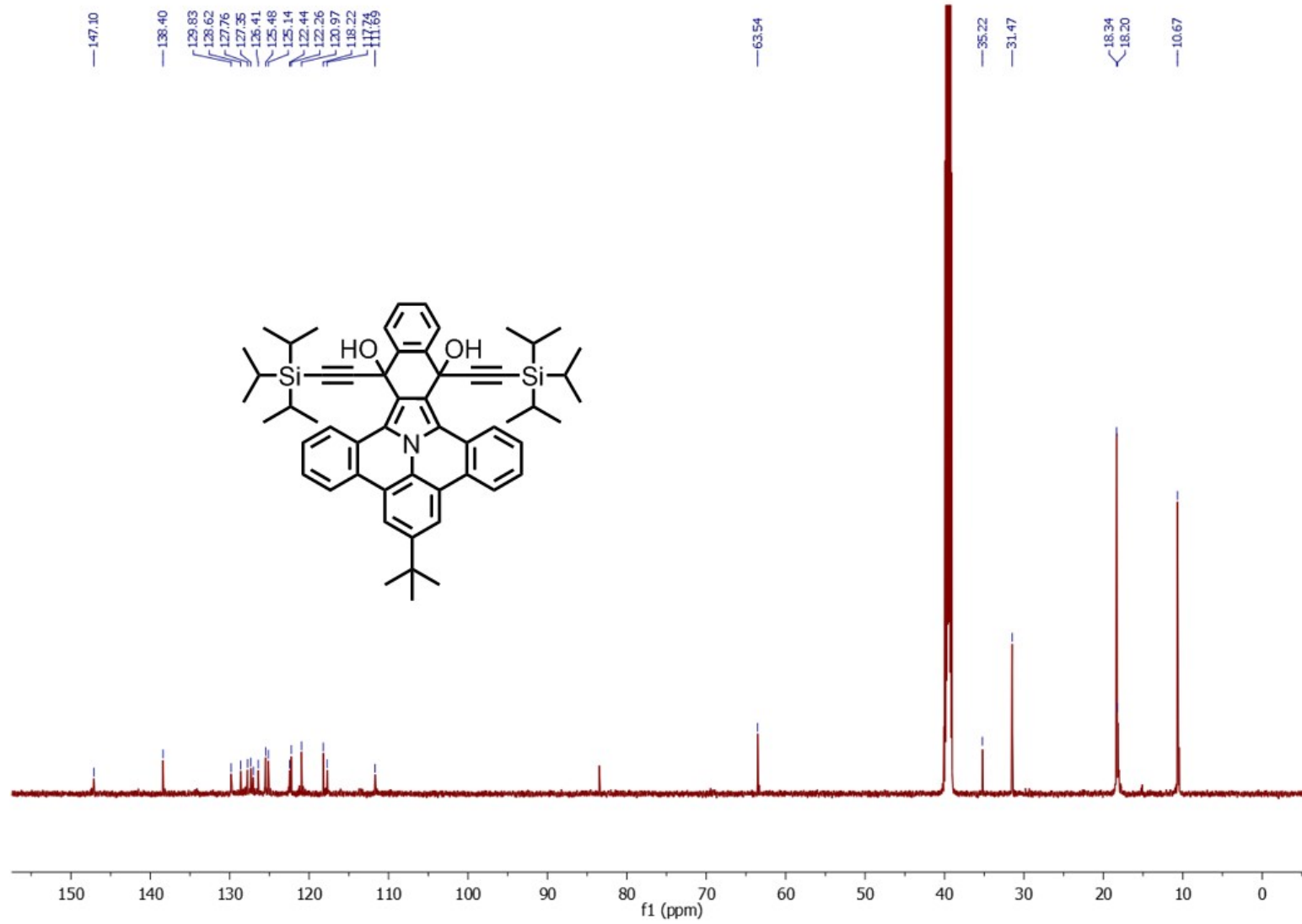


Figure S25. a) HR-MALDI-TOF spectrum of $1c^+$; b) HR-MALDI-TOF measurement of $1c^+$ (black line) is in agreement to the expected isotopic distribution pattern (red line).

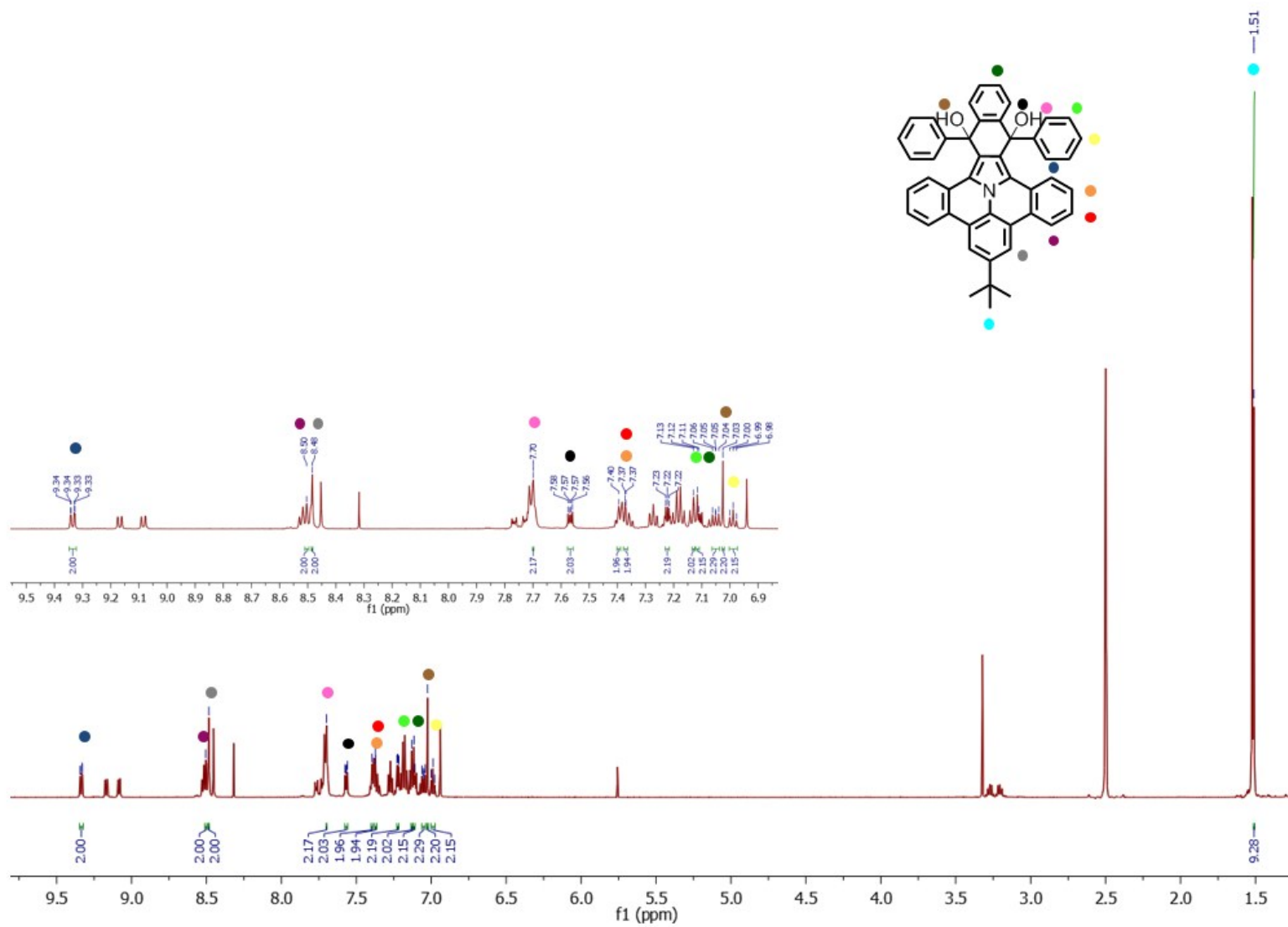
8) NMR Spectroscopy

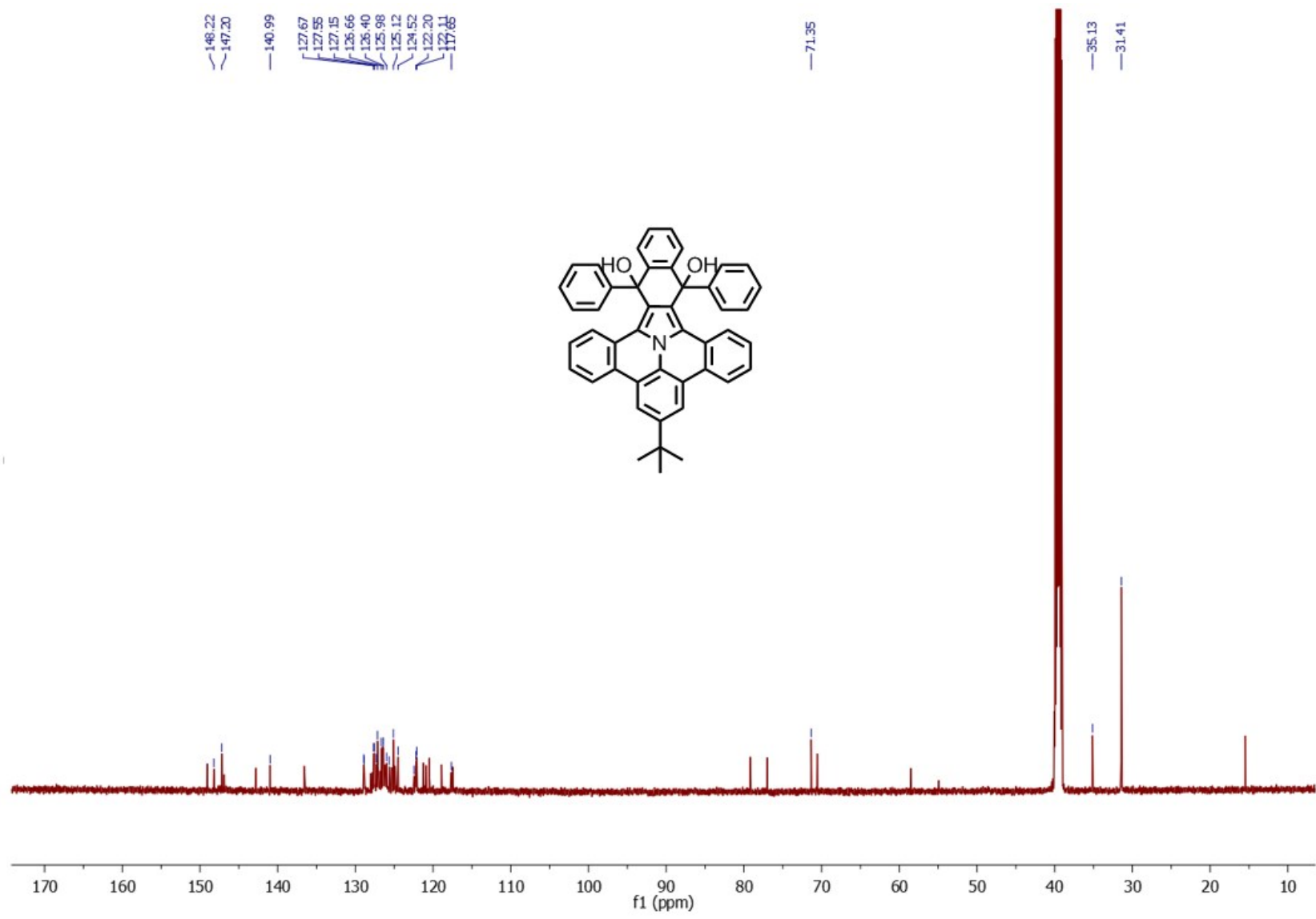
^1H -NMR (600 MHz, top) and ^{13}C -NMR (151 MHz, bottom) spectra of compound **3a** at 298 K in DMSO- d_6 .

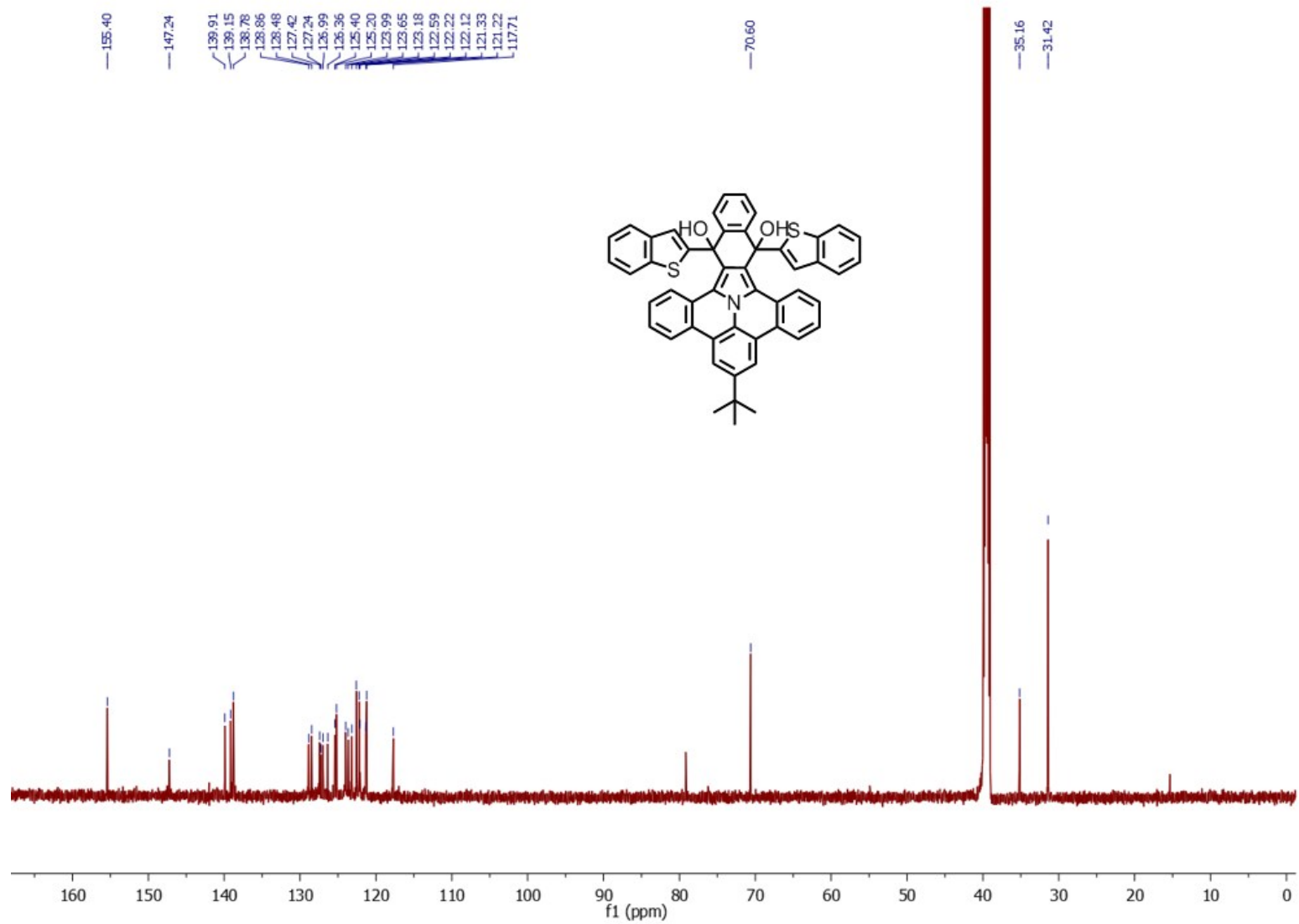




^1H -NMR (600 MHz, top) and ^{13}C -NMR (151 MHz, bottom) spectra of compound **3b** at 298 K in DMSO-d_6 .

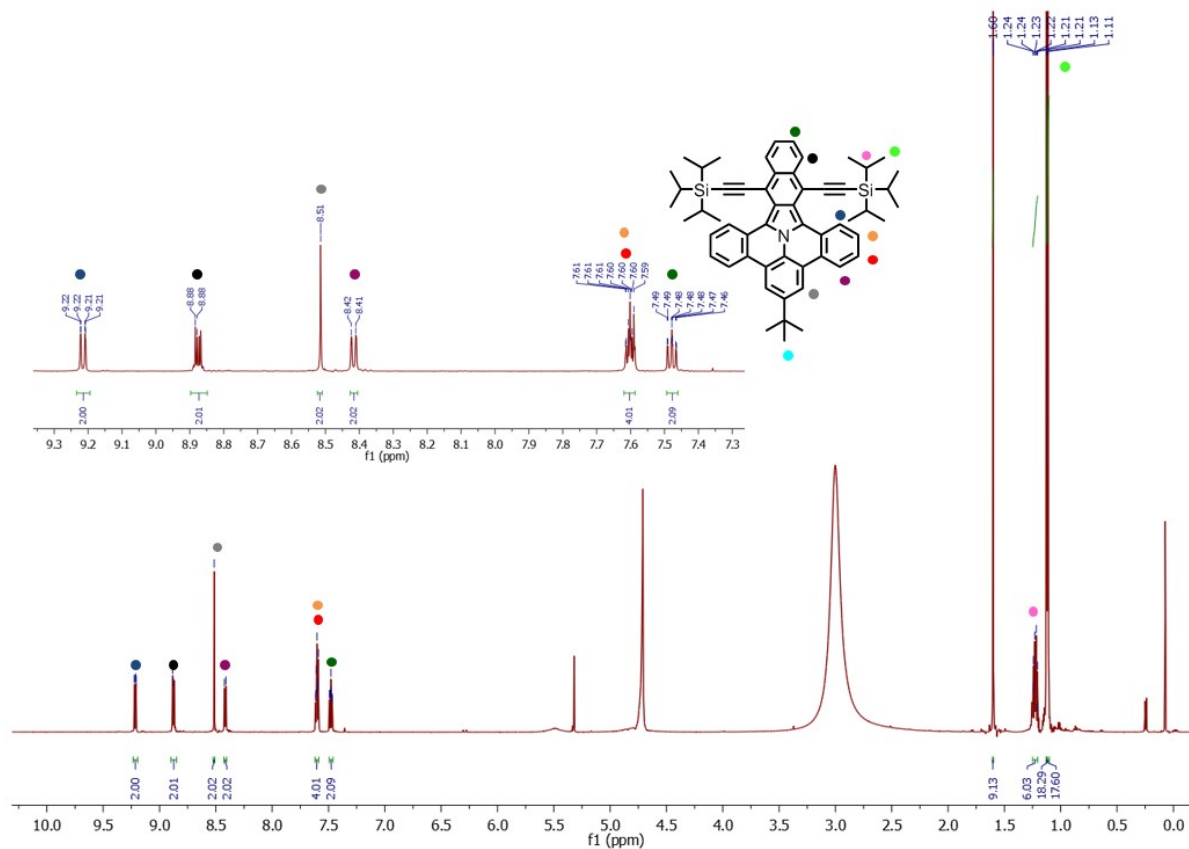


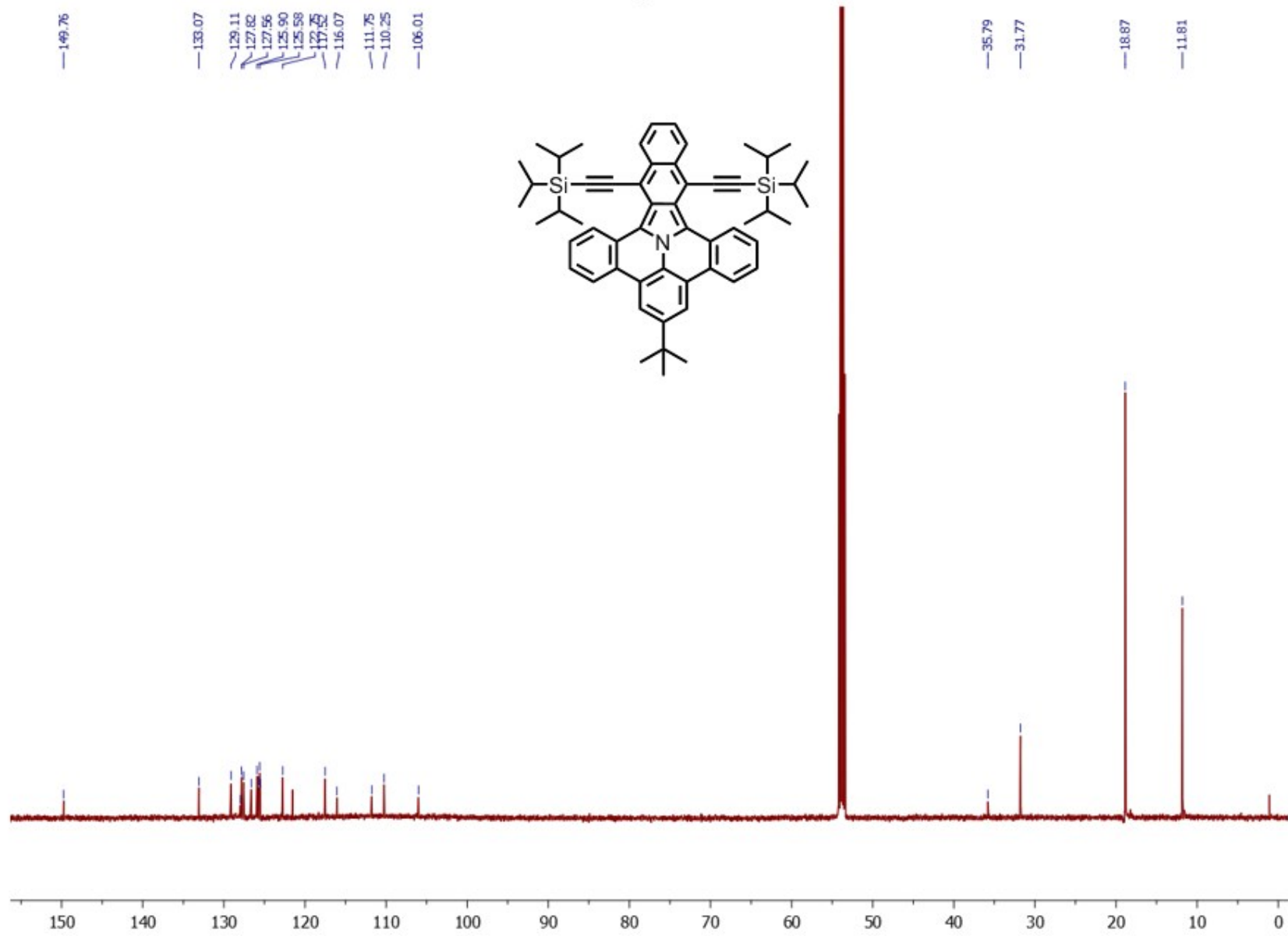




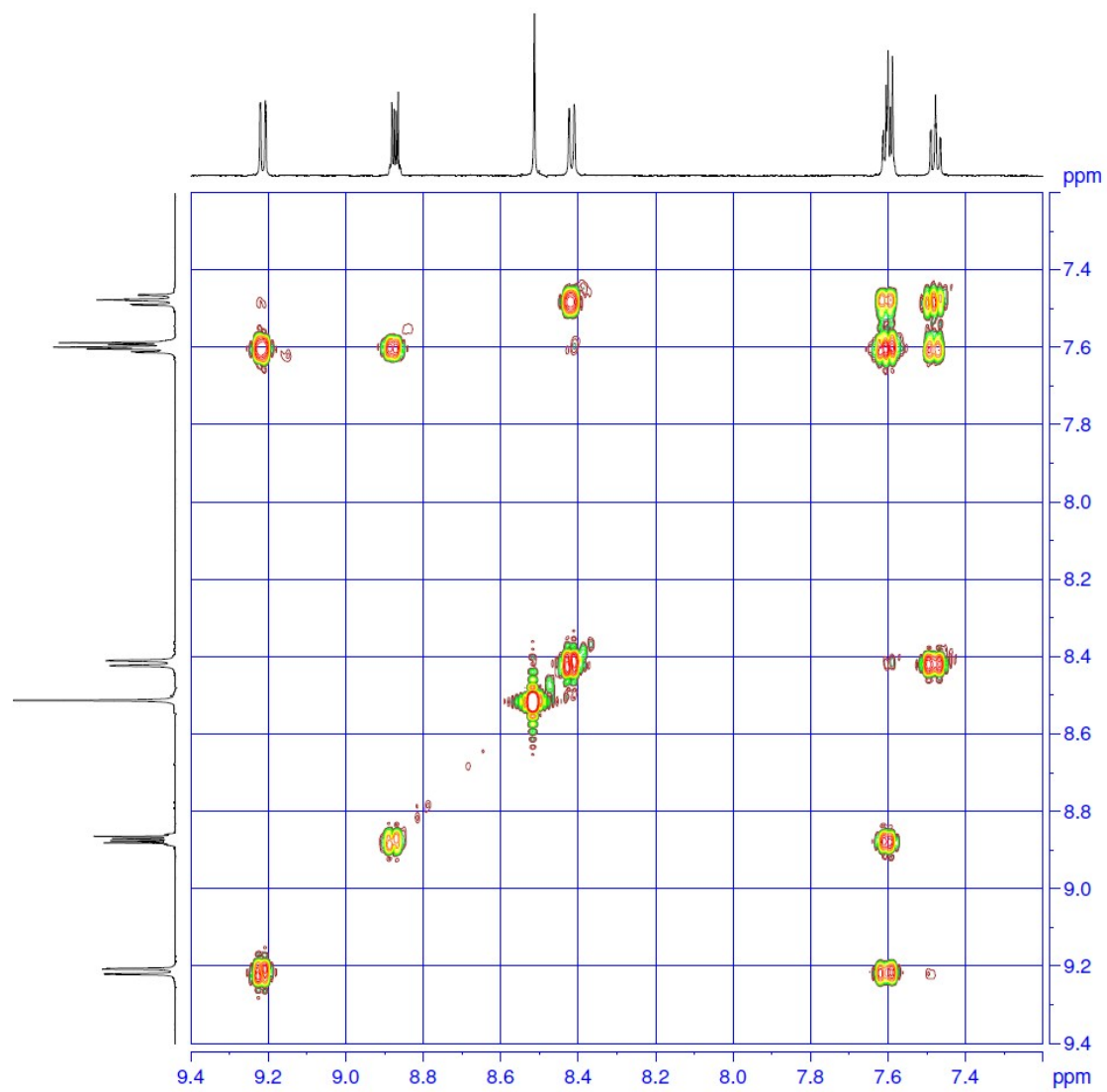
The ^1H -NMR spectra of **1a-c** showed broad signals in the aromatic region at room temperature. After the addition of the reducing agent hydrazine to quench radical impurities, sharp signals were observed in NMR spectra in d_2 -dichloromethane. The ^{13}C - and 2D-NMR spectra (Correlation spectroscopy (COSY), Heteronuclear Single Quantum Coherence (HSQC), Heteronuclear Multiple-Bond Correlation (HMBC), J-resolved spectroscopy (JERS) and Nuclear Overhauser Effect Spectroscopy (NOESY)) were further measured after addition of hydrazine.

^1H -NMR (600 MHz, top) and ^{13}C -NMR (151 MHz, bottom) spectra of compound **1a** at 298 K in DCM-d_2 .

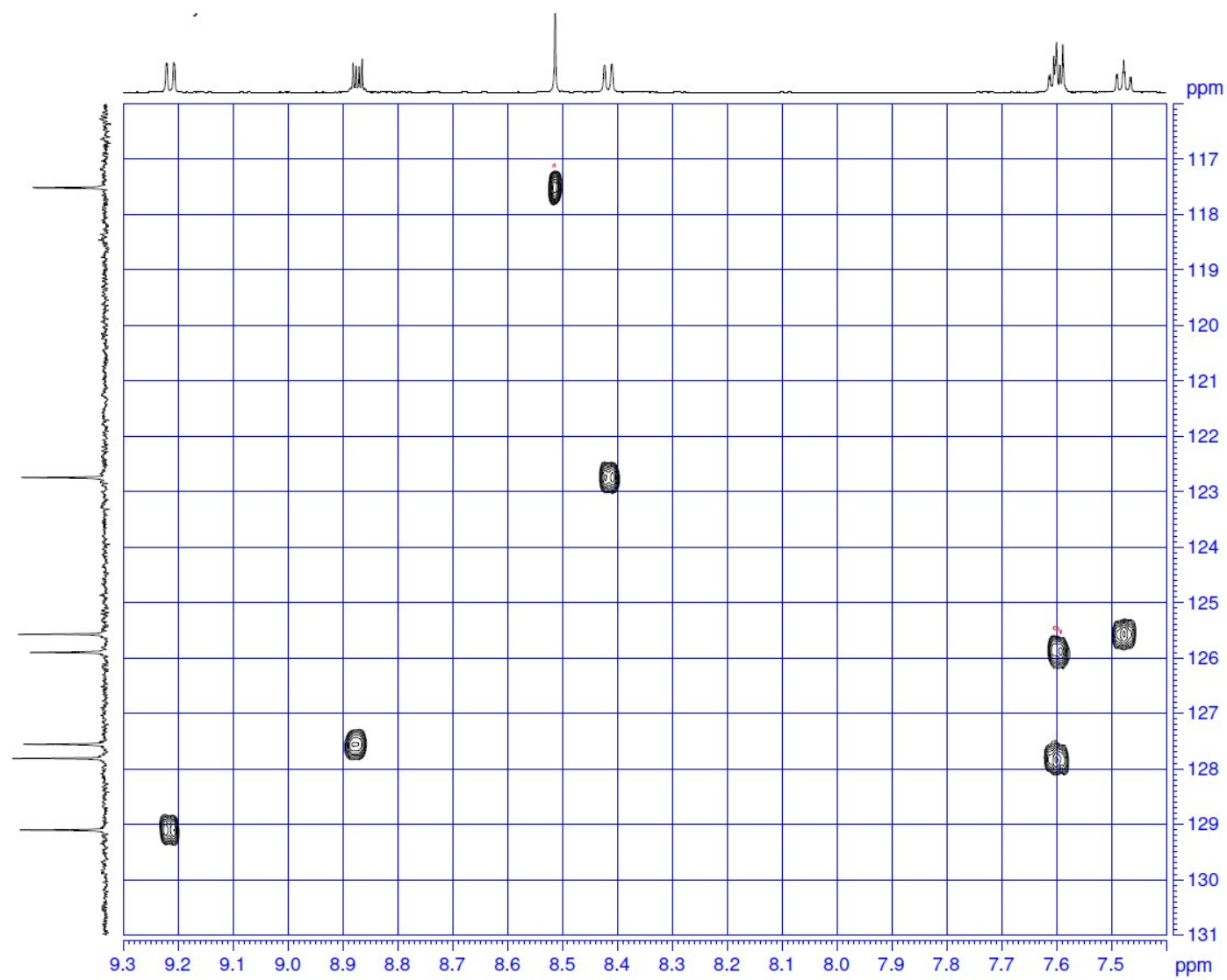




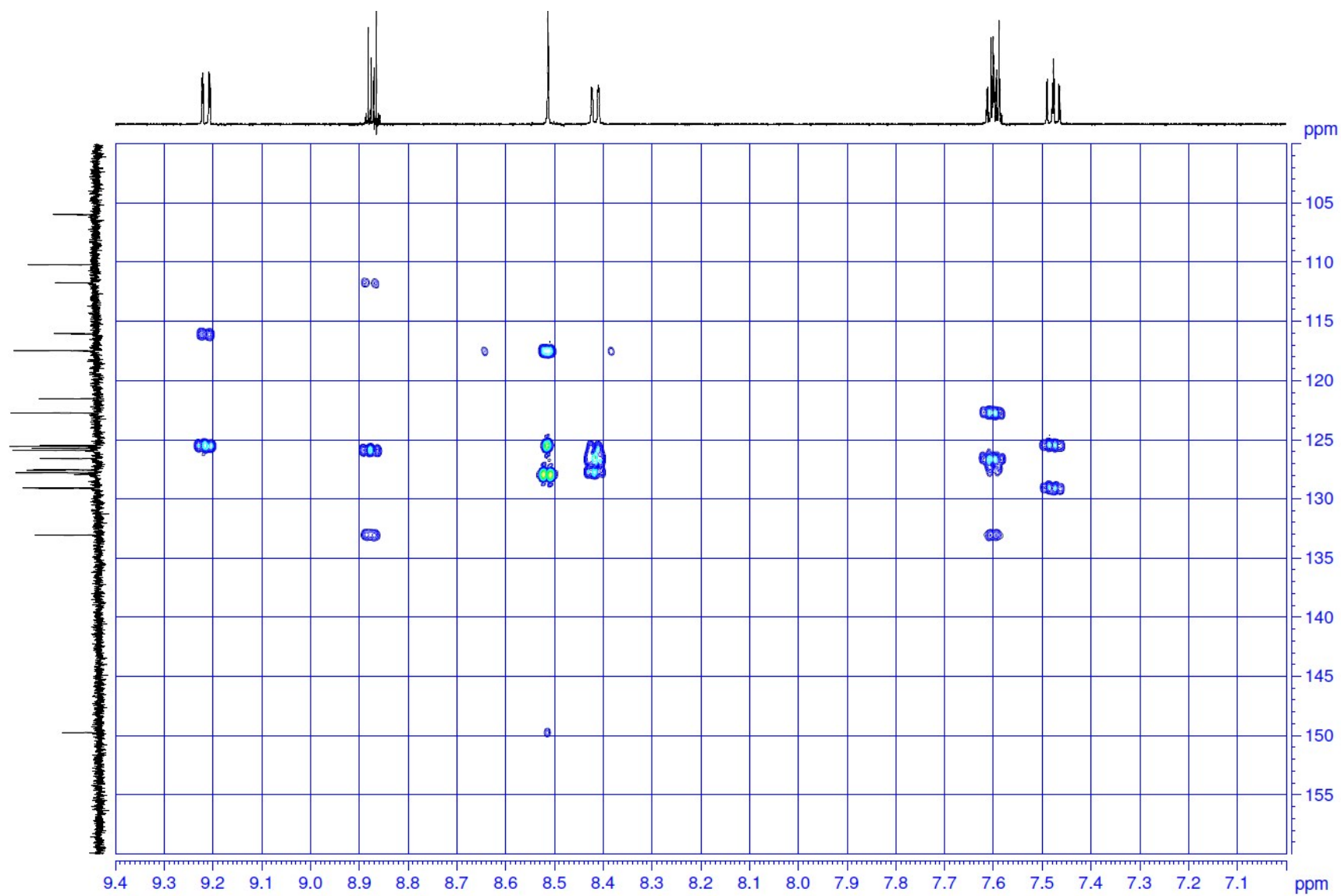
Correlation spectroscopy (COSY) of compound **1a**.



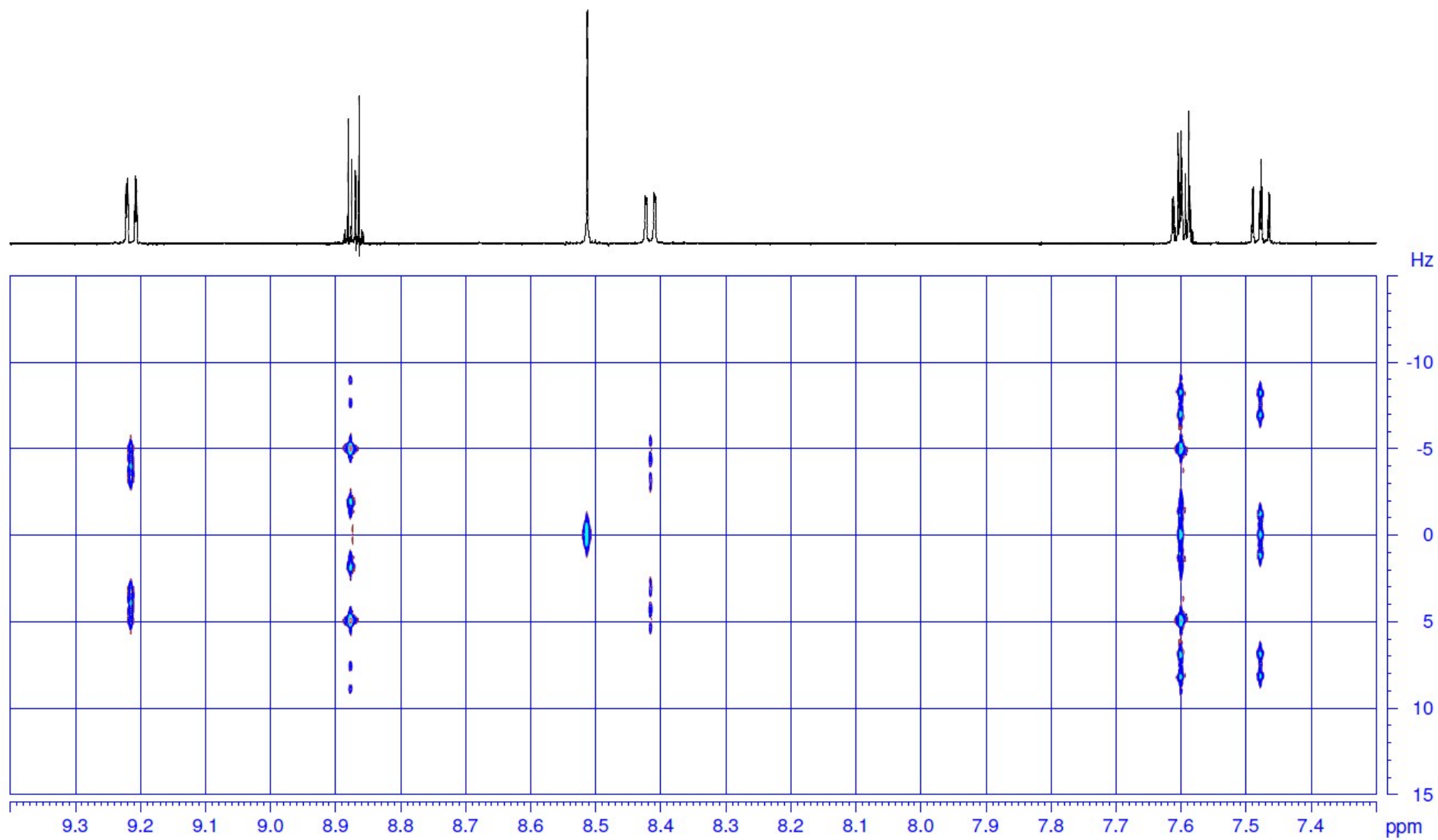
Heteronuclear Single Quantum Coherence (HSQC) of compound **1a**.



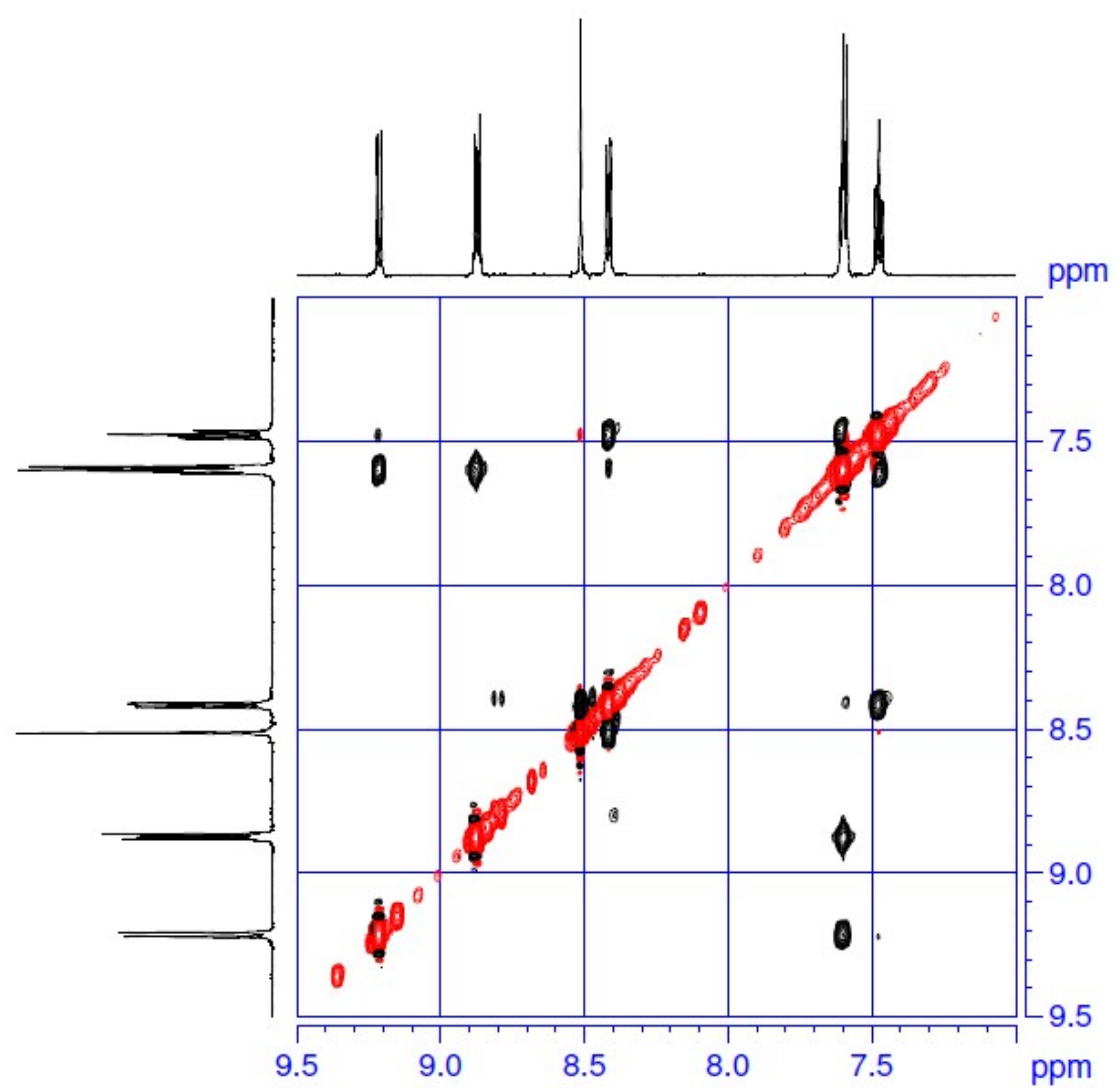
Heteronuclear Multiple-Bond Correlation (HMBC) of compound **1a**.



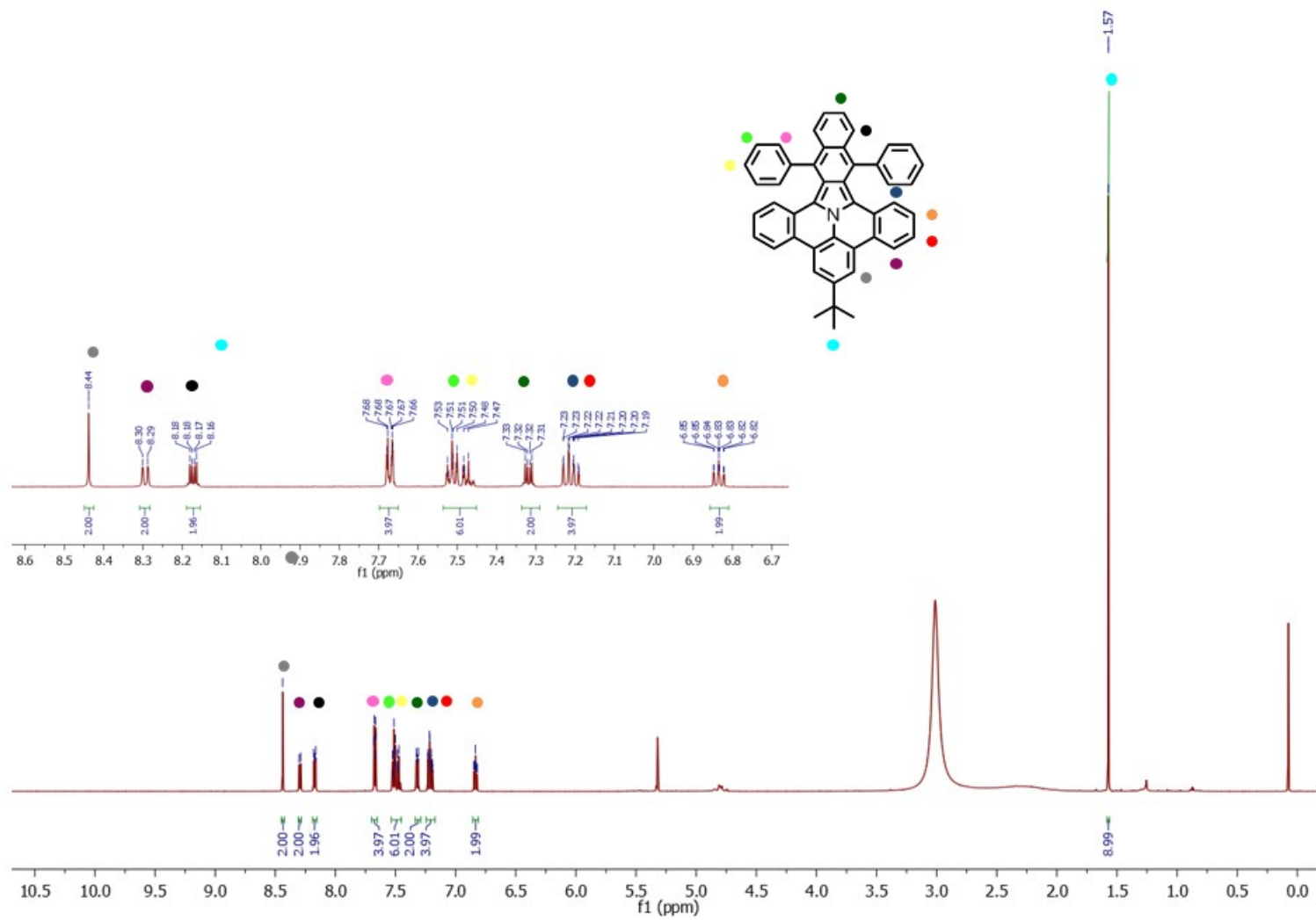
J-resolved spectroscopy (JERS) of compound **1a**.



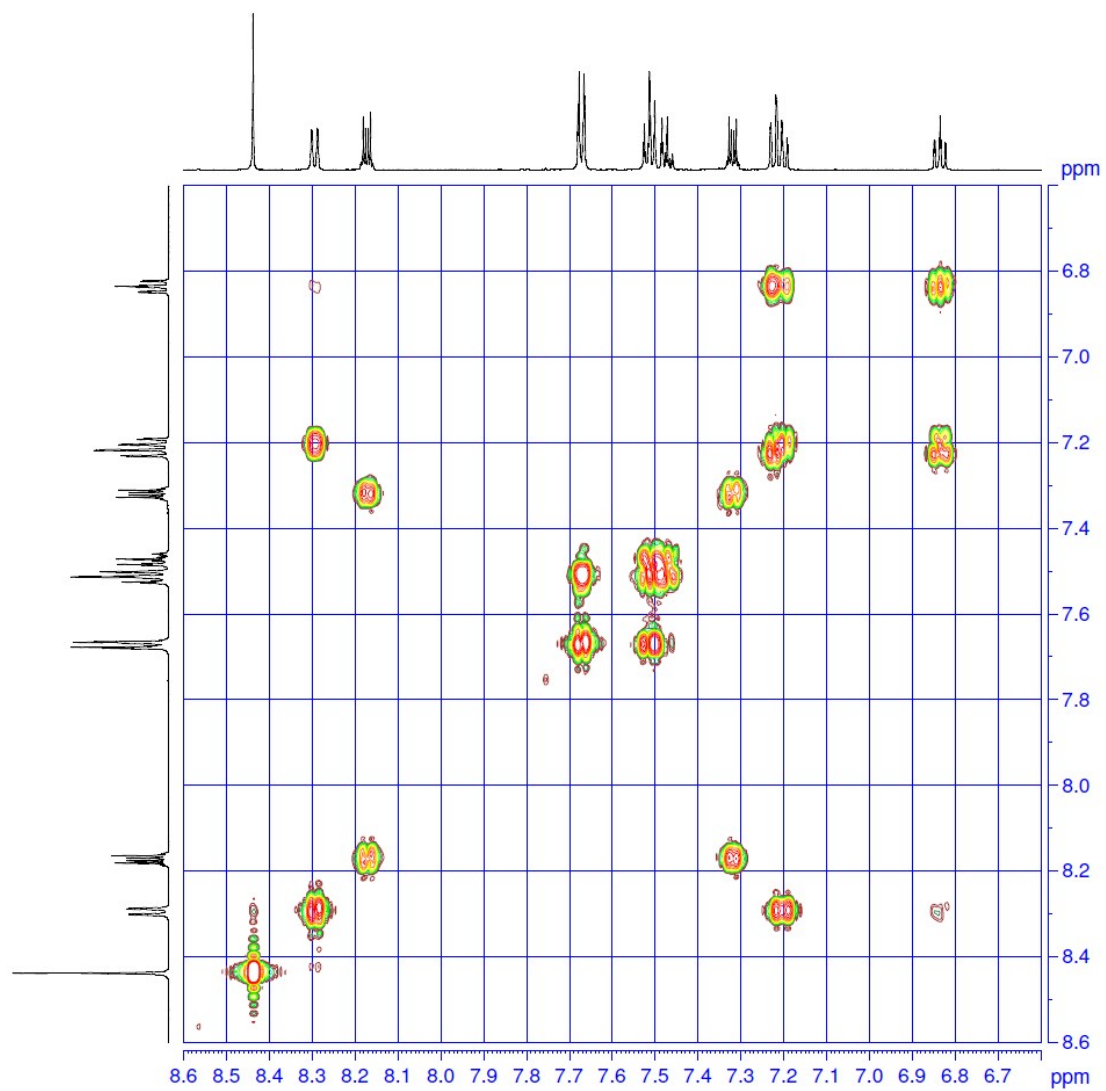
Nuclear Overhauser Effect Spectroscopy (NOESY) of compound **1a**.



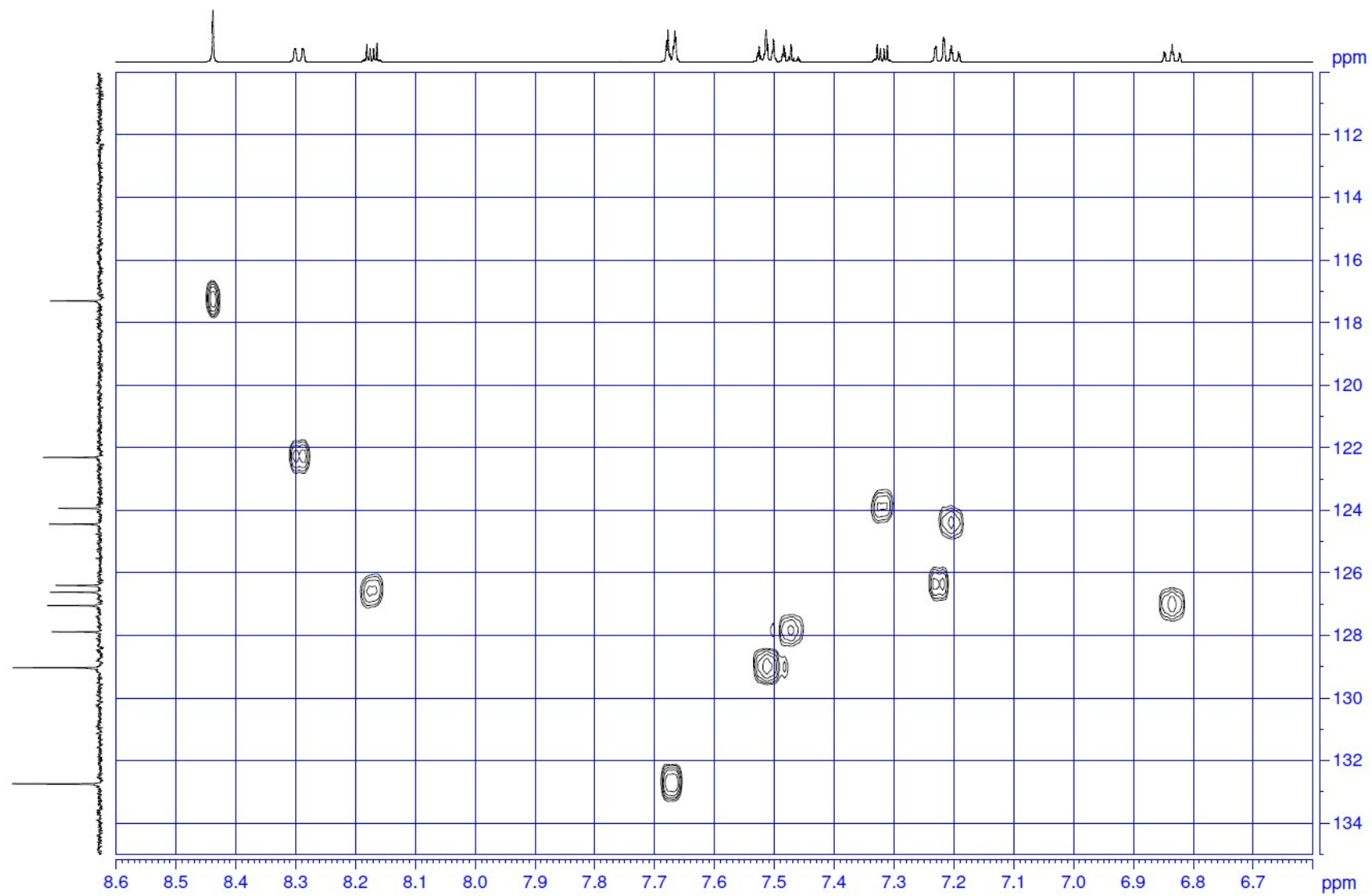
$^1\text{H-NMR}$ (600 MHz, top) and $^{13}\text{C-NMR}$ (151 MHz, bottom) spectra of compound **1b** at 298 K in DCM-d_2 .



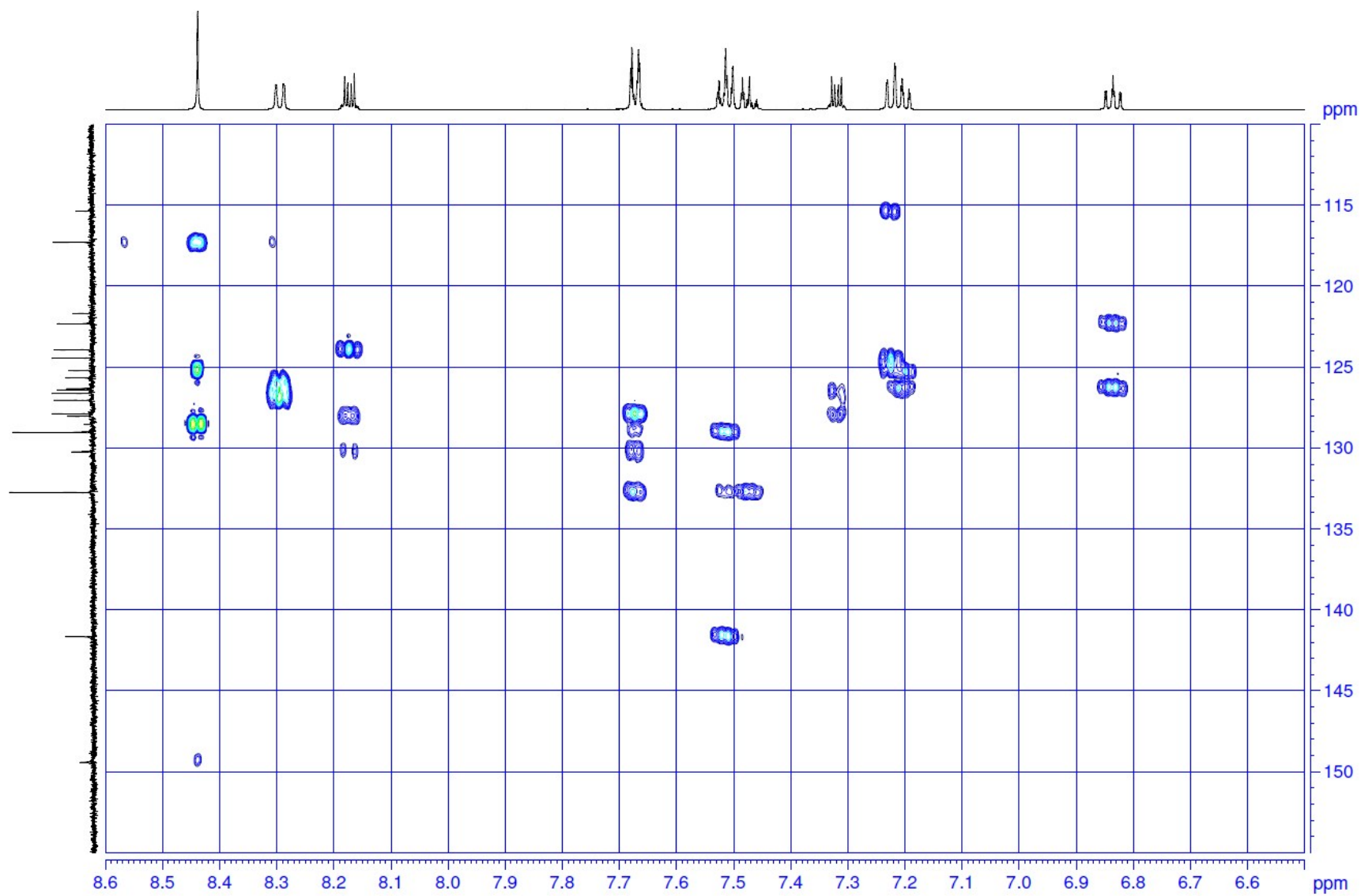
Correlation spectroscopy (COSY) of compound **1b**.



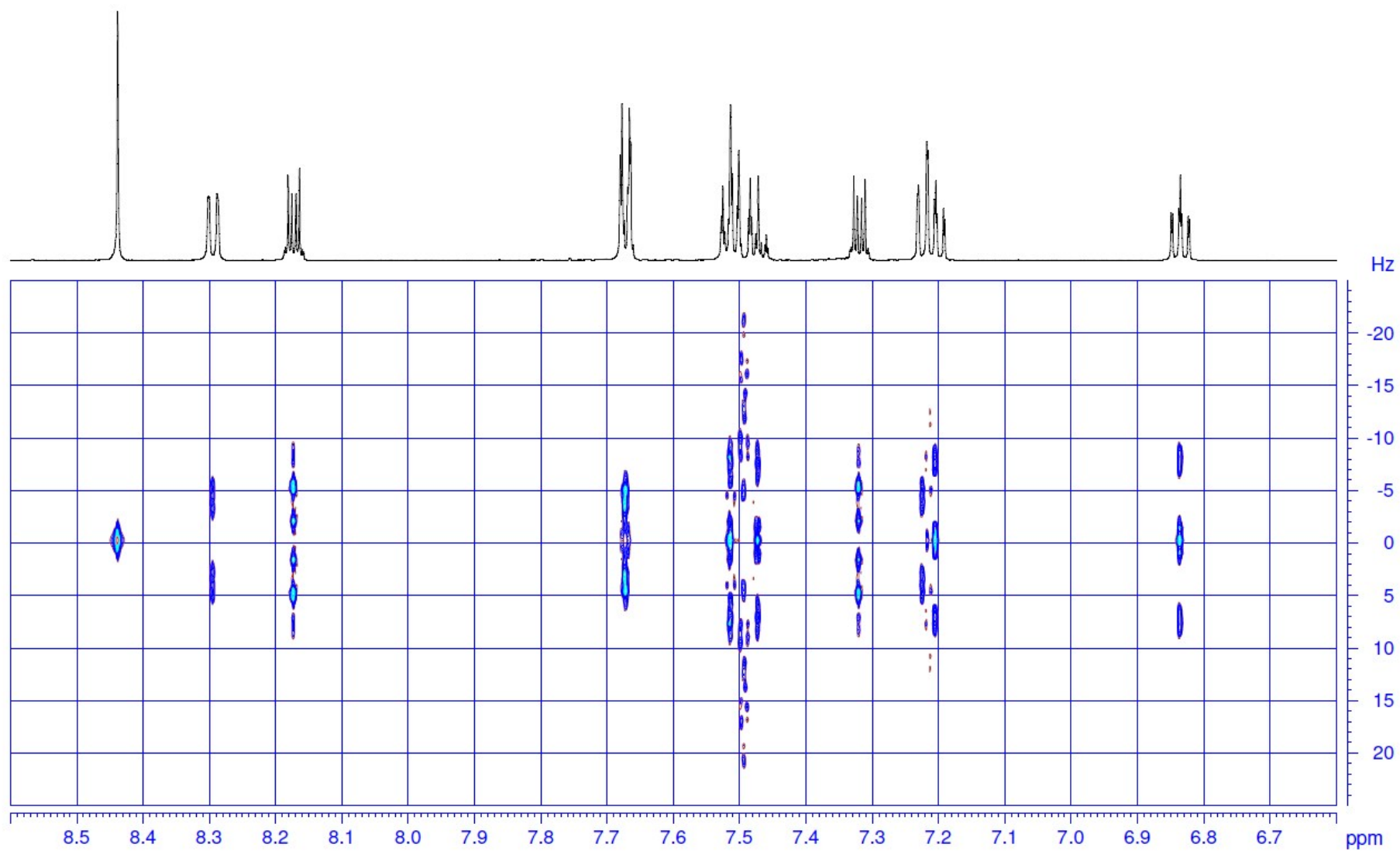
Heteronuclear Single Quantum Coherence (HSQC) of compound **1b**.



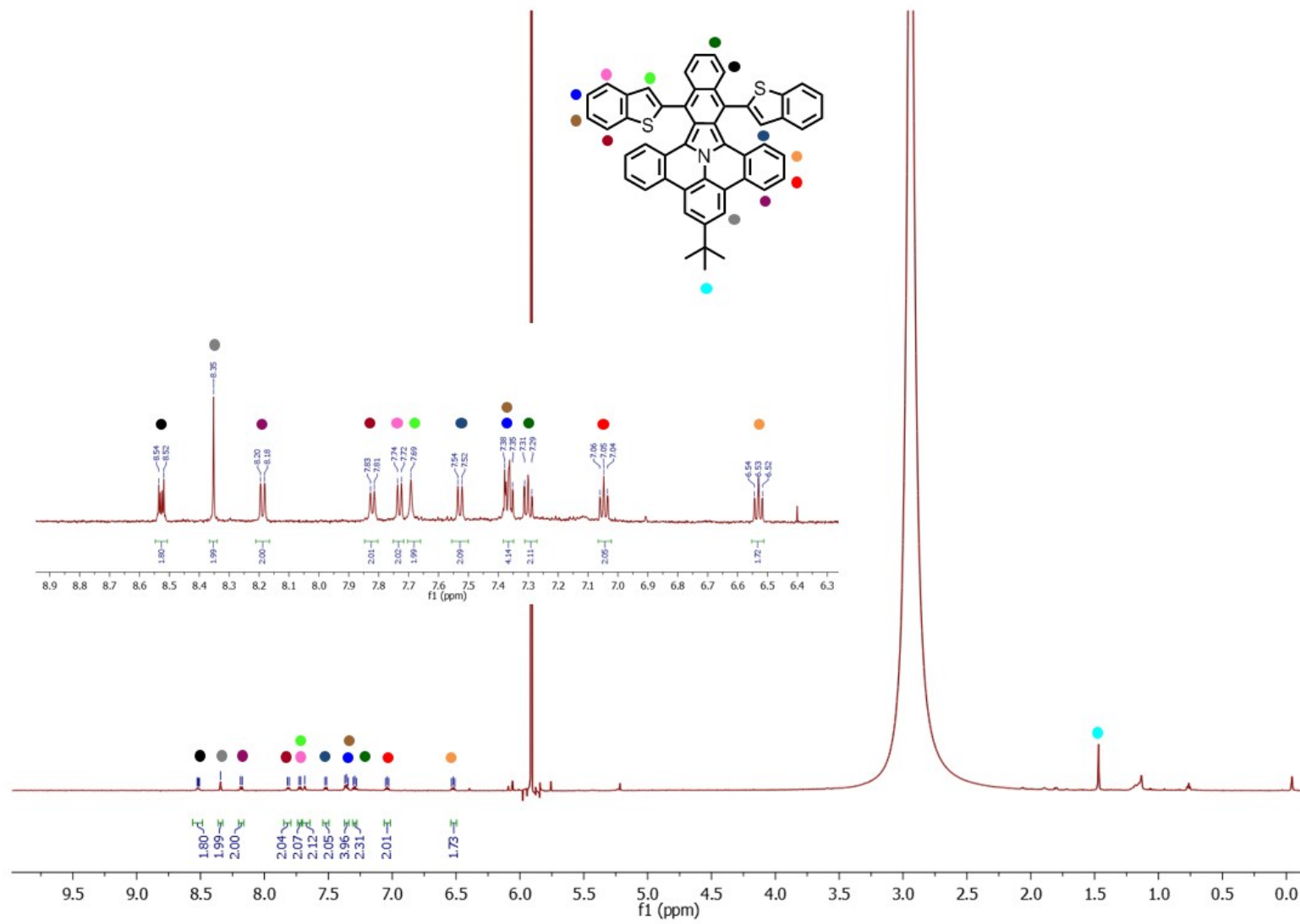
Heteronuclear Multiple-Bond Correlation (HMBC) of compound **1b**.



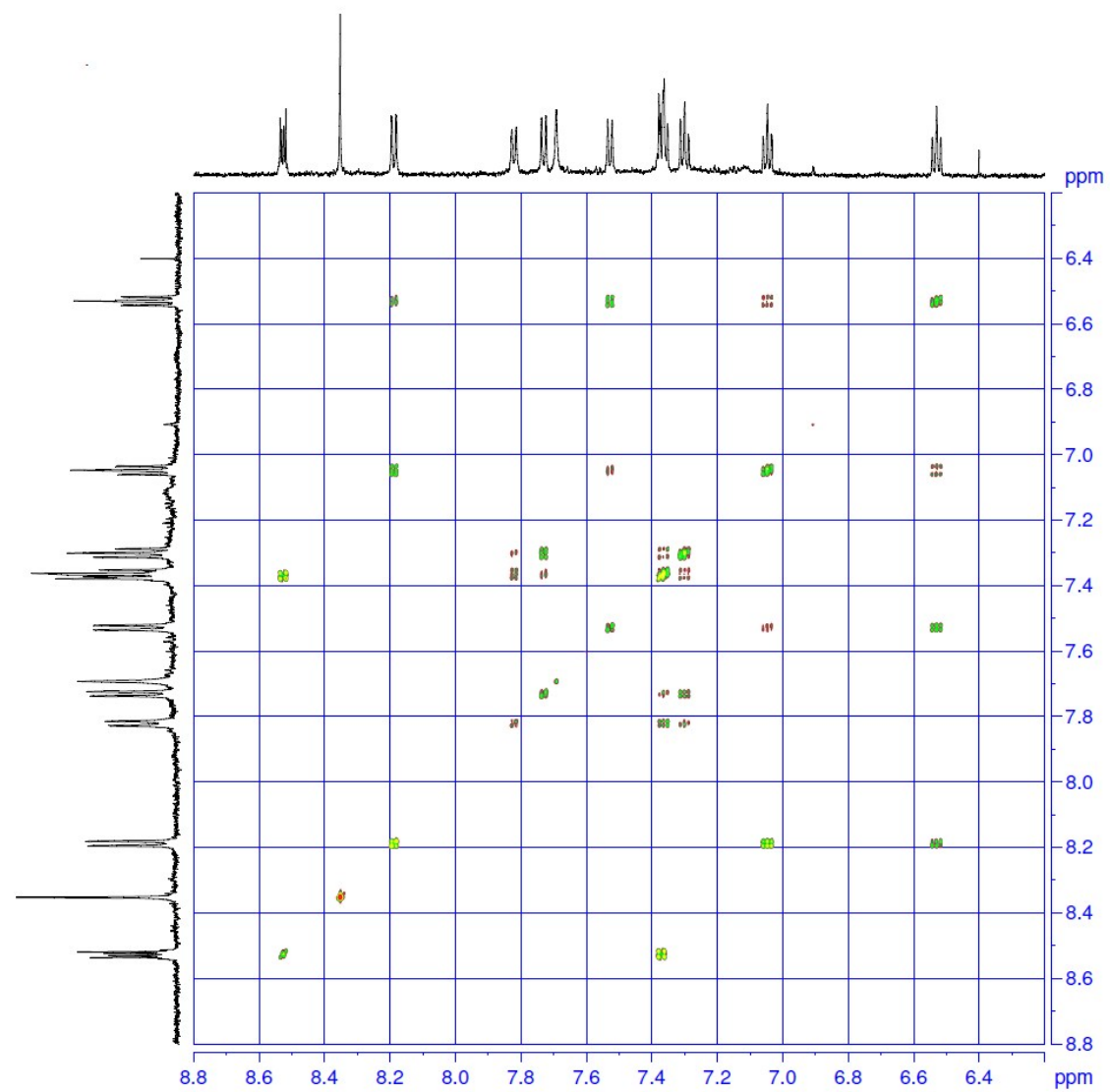
J-resolved spectroscopy (JERS) of compound **1b**.



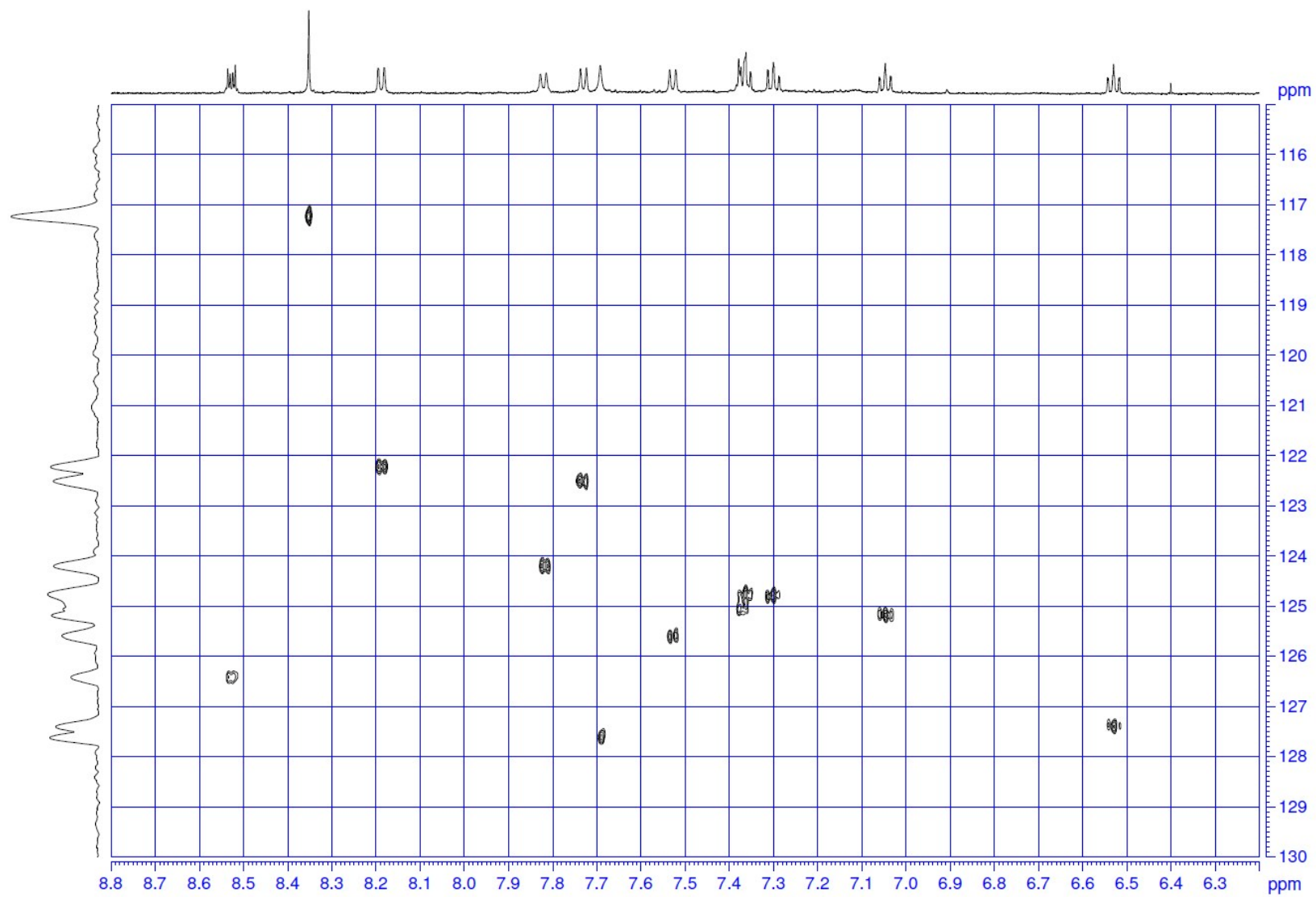
$^1\text{H-NMR}$ (600 MHz) spectra of compound **1c** at 298 K in CD_2Cl_4 .



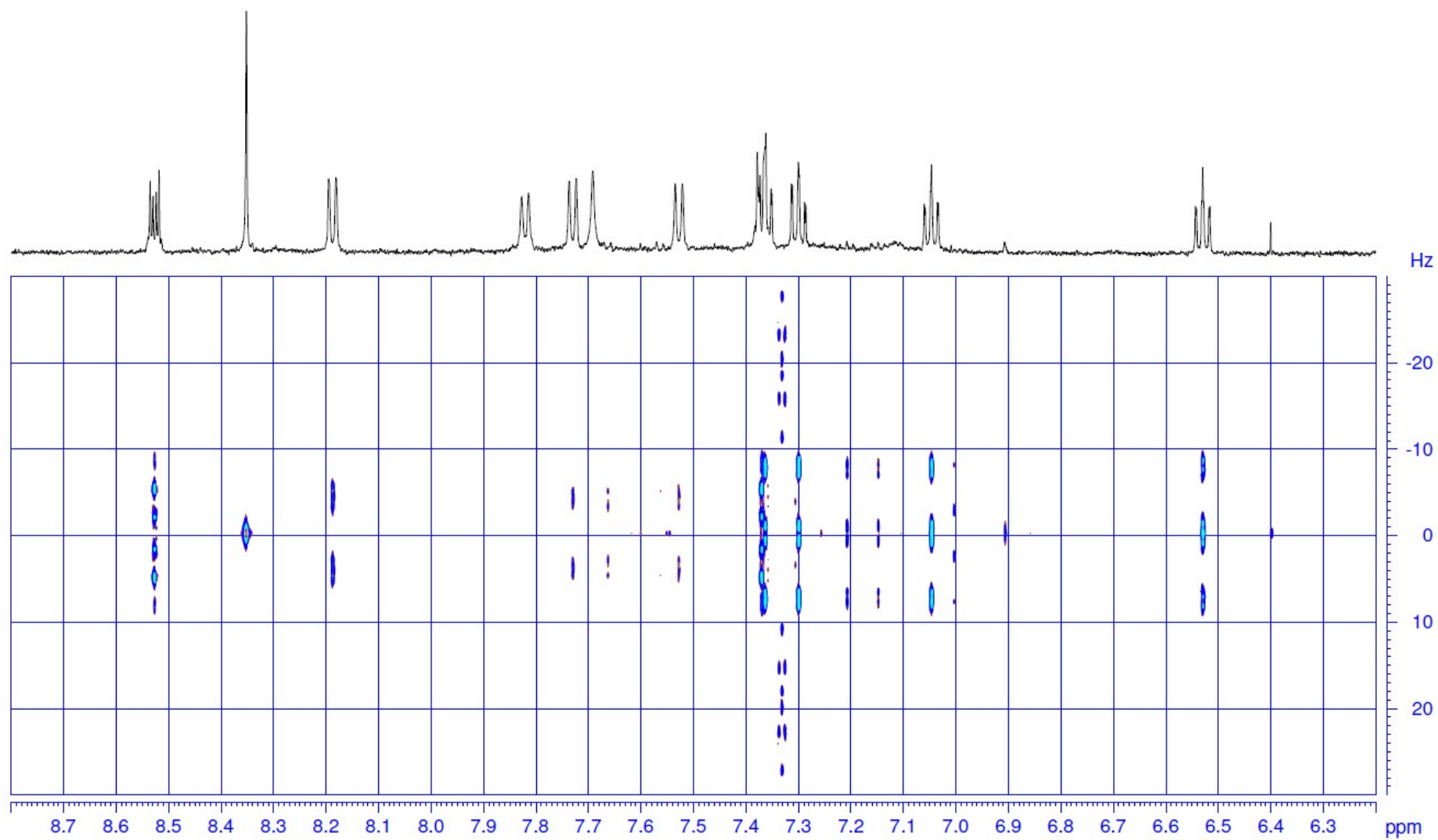
Correlation spectroscopy (COSY) of compound **1c**.



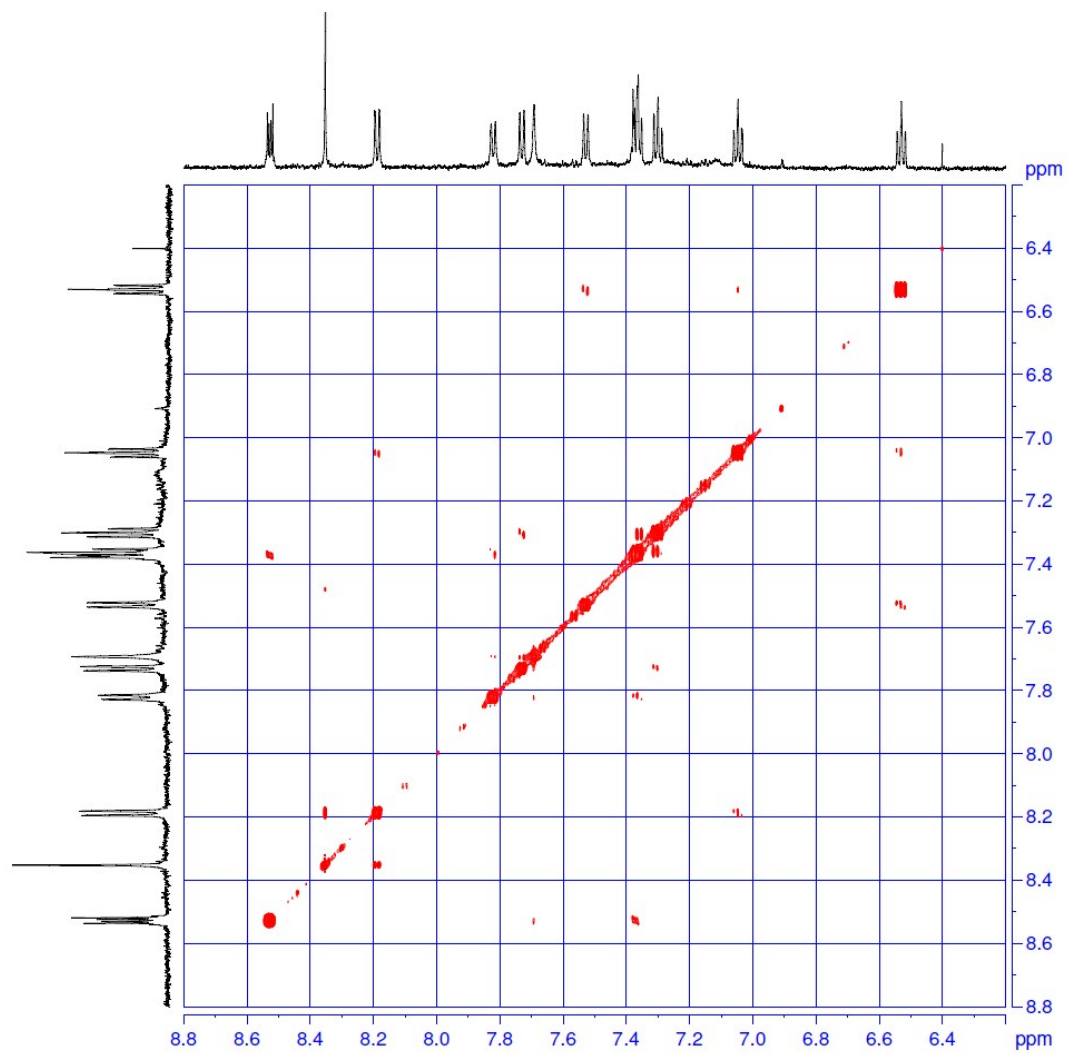
Heteronuclear Single Quantum Coherence (HSQC) of compound **1c**.



J-resolved spectroscopy (JERS) of compound **1c**.



Nuclear Overhauser Effect Spectroscopy (NOESY) of compound **1c**.



12) References

1. R. Berger, M. Wagner, X. Feng and K. Müllen, *Chem. Sci.*, 2015, **6**, 436-441.
2. M. J. T. Frisch, G. W.; Schlegel, H. B.; Scuseria, G. E.; Robb, M. A.; Cheeseman, J. R.; Scalmani, G.; Barone, V.; Mennucci, B.; Petersson, G. A.; Nakatsuji, H.; Caricato, M.; Li, X.; Hratchian, H. P.; Izmaylov, A. F.; Bloino, J.; Zheng, G.; Sonnenberg, J. L.; Hada, M.; Ehara, M.; Toyota, K.; Fukuda, R.; Hasegawa, J.; Ishida, M.; Nakajima, T.; Honda, Y.; Kitao, O.; Nakai, H.; Vreven, T.; Montgomery, Jr., J. A.; Peralta, J. E.; Ogliaro, F.; Bearpark, M.; Heyd, J. J.; Brothers, E.; Kudin, K. N.; Staroverov, V. N.; Kobayashi, R.; Normand, J.; Raghavachari, K.; Rendell, A.; Burant, J. C.; Iyengar, S. S.; Tomasi, J.; Cossi, M.; Rega, N.; Millam, N. J.; Klene, M.; Knox, J. E.; Cross, J. B.; Bakken, V.; Adamo, C.; Jaramillo, J.; Gomperts, R.; Stratmann, R. E.; Yazyev, O.; Austin, A. J.; Cammi, R.; Pomelli, C.; Ochterski, J. W.; Martin, R. L.; Morokuma, K.; Zakrzewski, V. G.; Voth, G. A.; Salvador, P.; Dannenberg, J. J.; Dapprich, S.; Daniels, A. D.; Farkas, Ö.; Foresman, J. B.; Ortiz, J. V.; Cioslowski, J., *D. J. Gaussian Inc.*, 2009, **Wallingford CT**.
3. T. Yanai, D. P. Tew and N. C. Handy, *Chemical Physics Letters*, 2004, **393**, 51-57.
4. R. Krishnan, J. S. Binkley, R. Seeger and J. A. Pople, *The Journal of Chemical Physics*, 1980, **72**, 650-654.
5. X. Wang, F. Zhang, K. S. Schellhammer, P. Machata, F. Ortmann, G. Cuniberti, Y. Fu, J. Hunger, R. Tang, A. A. Popov, R. Berger, K. Müllen and X. Feng, *Journal of the American Chemical Society*, 2016, **138**, 11606-11615.
6. K. Yamaguchi, F. Jensen, A. Dorigo and K. N. Houk, *Chemical Physics Letters*, 1988, **149**, 537-542.
7. K. Yamaguchi, Y. Takahara, T. Fueno and K. N. Houk, *Theoretica chimica acta*, 1988, **73**, 337-364.
8. D. Hegarty and M. A. Robb, *Molecular Physics*, 1979, **38**, 1795-1812.
9. R. H. A. Eade and M. A. Robb, *Chemical Physics Letters*, 1981, **83**, 362-368.
10. H. B. Schlegel and M. A. Robb, *Chemical Physics Letters*, 1982, **93**, 43-46.
11. F. Bernardi, A. Bottoni, J. J. W. McDouall, M. A. Robb and H. B. Schlegel, *Faraday Symposia of the Chemical Society*, 1984, **19**, 137-147.
12. M. Frisch, I. N. Ragazos, M. A. Robb and H. Bernhard Schlegel, *Chemical Physics Letters*, 1992, **189**, 524-528.
13. N. Yamamoto, T. Vreven, M. A. Robb, M. J. Frisch and H. Bernhard Schlegel, *Chemical Physics Letters*, 1996, **250**, 373-378.
14. M. Head-Gordon, *Chemical Physics Letters*, 2003, **372**, 508-511.
15. T. Koide, K. Furukawa, H. Shinokubo, J.-Y. Shin, K. S. Kim, D. Kim and A. Osuka, *Journal of the American Chemical Society*, 2010, **132**, 7246-7247.
16. A. Das, T. Müller, F. Plasser and H. Lischka, *The Journal of Physical Chemistry A*, 2016, **120**, 1625-1636.
17. A. Konishi, Y. Hirao, M. Nakano, A. Shimizu, E. Botek, B. Champagne, D. Shiomi, K. Sato, T. Takui, K. Matsumoto, H. Kurata and T. Kubo, *Journal of the American Chemical Society*, 2010, **132**, 11021-11023.
18. A. Shimizu, Y. Hirao, K. Matsumoto, H. Kurata, T. Kubo, M. Uruichi and K. Yakushi, *Chemical Communications*, 2012, **48**, 5629-5631.